

CERN-EP-2017-112
2017/10/10

CMS-TOP-14-008

Measurement of the semileptonic $t\bar{t} + \gamma$ production cross section in pp collisions at $\sqrt{s} = 8$ TeV

The CMS Collaboration*

Abstract

A measurement of the cross section for top quark-antiquark ($t\bar{t}$) pairs produced in association with a photon in proton-proton collisions at $\sqrt{s} = 8$ TeV is presented. The analysis uses data collected with the CMS detector at the LHC, corresponding to an integrated luminosity of 19.7 fb^{-1} . The signal is defined as the production of a $t\bar{t}$ pair in association with a photon having a transverse energy larger than 25 GeV and an absolute pseudorapidity smaller than 1.44. The measurement is performed in the fiducial phase space corresponding to the semileptonic decay chain of the $t\bar{t}$ pair, and the cross section is measured relative to the inclusive $t\bar{t}$ pair production cross section. The fiducial cross section for associated $t\bar{t}$ pair and photon production is found to be 127 ± 27 (stat+syst) fb per semileptonic final state. The measured value is in agreement with the theoretical prediction.

Published in the Journal of High Energy Physics as doi:10.1007/JHEP10(2017)006.

arXiv:1706.08128v2 [hep-ex] 9 Oct 2017

1 Introduction

As the heaviest elementary particle in the standard model (SM), the top quark has the potential to provide insights into physics beyond the SM (BSM). Many BSM models introduce changes within the top quark sector [1, 2], which can be constrained by precise measurements of the cross sections and properties of top quark production channels [3]. By measuring the associated production cross section of a top quark-antiquark pair and a photon ($t\bar{t}+\gamma$), the coupling of the top quark and the photon is probed [4, 5]. Any deviation of the measured cross section value from the SM prediction would be an indication of BSM physics, such as the production of an exotic quark with electric charge of $-4/3$, or a top quark with an anomalous electric dipole moment [6, 7].

As the top quark predominantly decays to a W boson and a b quark, the $t\bar{t}+\gamma$ production can be identified by the presence of a photon candidate and the decay products of a pair of top quarks, namely two jets from the hadronization of two b quarks, and the decay products of a pair of W bosons. In this analysis, events are selected in which one W boson decays leptonically, resulting in an electron or muon and a corresponding neutrino ν , and the other W boson decays hadronically. Examples of two Feynman diagrams for the $t\bar{t}+\gamma$ process in the semileptonic final states are shown in Fig. 1. In the signal definition we include possible contributions from $W \rightarrow \tau\nu_\tau$, where the τ lepton decays further into an electron or a muon. The presence of a charged lepton from the W boson decay significantly improves the power to reject dominant backgrounds from multijet processes and allows for efficient triggering of signal events using single-lepton triggers.

Measurements of the production cross section of $t\bar{t}+\gamma$ have been performed by the CDF Collaboration at the Tevatron using $p\bar{p}$ collisions at $\sqrt{s} = 1.96$ TeV [8], and by the ATLAS Collaboration at the LHC using pp collisions at $\sqrt{s} = 7$ TeV [9] and $\sqrt{s} = 8$ TeV [10]. These results are in agreement with the SM predictions within uncertainties [11].

In this paper, the measurement of the $t\bar{t}+\gamma$ production cross section in pp collisions at $\sqrt{s} = 8$ TeV is presented. The analysis is based on a data sample corresponding to an integrated luminosity of 19.7 fb^{-1} , recorded with the CMS detector in 2012. The measurement of the $t\bar{t}+\gamma$ production cross section in the semileptonic decay channel is performed relative to the $t\bar{t}$ production cross section. The $t\bar{t}+\gamma$ cross section is measured in a fiducial kinematic region defined by the presence of exactly one charged lepton and corresponding neutrino, at least three jets, and a photon within the selection requirements.

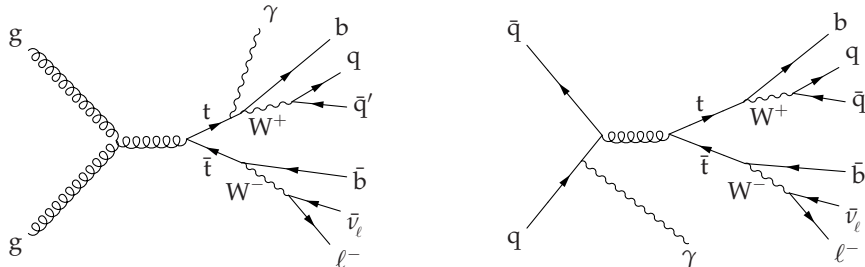


Figure 1: Dominant Feynman diagrams for the $t\bar{t}+\gamma$ signal process in the semileptonic final state where the $t\bar{t}$ pair is produced through gluon-gluon fusion with a photon emitted from one of the top quarks (left), and through quark-antiquark annihilation with a photon emitted from one of the initial partons (right).

2 The CMS detector

The central feature of the CMS apparatus is a superconducting solenoid of 6 m internal diameter, providing a magnetic field of 3.8 T. Within the solenoid volume are a silicon pixel and strip tracker, a lead tungstate crystal electromagnetic calorimeter (ECAL), and a brass and scintillator hadron calorimeter, each composed of a barrel and two endcap sections. Forward calorimeters extend the pseudorapidity η coverage provided by the barrel and endcap detectors. Muons are detected in gas-ionization chambers embedded in the steel flux-return yoke outside the solenoid. In the barrel section of the ECAL, an energy resolution of about 1% is achieved for unconverted or late-converting photons in the tens of GeV energy range, relevant to this analysis. The remaining barrel photons have a resolution of about 1.3% up to $|\eta| = 1$, rising to about 2.5% at $|\eta| = 1.4$. In the endcaps, the resolution of unconverted or late-converting photons is about 2.5%, while the remaining endcap photons have a resolution between 3 and 4% [12]. A more detailed description of the CMS detector, together with a definition of the coordinate system used and the relevant kinematic variables, can be found in Ref. [13].

3 Signal and background modeling

The signal process produces events in which a pair of top quarks is produced in association with a photon. This process includes photons radiated from the top quarks as well as from initial state partons or the decay products of the top quarks. The simulation of the $t\bar{t}+\gamma$ signal process is performed in the region with photons having transverse momentum (p_T) of at least 13 GeV and $|\eta| < 3.0$, as well as having a separation from all other generated particles of at least $\Delta R > 0.3$, where $\Delta R = \sqrt{(\Delta\phi)^2 + (\Delta\eta)^2}$, and $\Delta\phi$ and $\Delta\eta$ are the differences in the azimuthal angle (in radians) and pseudorapidity, respectively, between the generated particles and the photon. For the purpose of this analysis, nonprompt photons originating from jets are not included in the definition of the $t\bar{t}+\gamma$ signal process.

The $t\bar{t}+\gamma$ signal process is simulated at leading order (LO) using the MADGRAPH v5.1.3.30 generator [14]. The dominant backgrounds, $t\bar{t}$, V +jets, and $V+\gamma$ (where $V = W, Z$), are also simulated using the MADGRAPH generator. Single top quark production is simulated at next-to-leading order (NLO) using the POWHEG v1.0 r1380 event generator [15–18]. In order to avoid any overlap between the simulation of the $t\bar{t}+\gamma$ signal and the inclusive $t\bar{t}$ process, events that fall under the $t\bar{t}+\gamma$ signal definition are removed from $t\bar{t}$ simulation. Overlap between $V+\gamma$ and V +jets simulation is also taken into account by removing events from V +jets samples, which are accounted for in the $V+\gamma$ simulation. Approximately 1% of events from $t\bar{t}$ simulation and approximately 3% of V +jets events are removed through this procedure.

The parton showering and hadronization for all simulated samples are handled by PYTHIA v6.426 [19], with the decays of τ leptons modeled with TAUOLA v27.121.5 [20]. The CTEQ6L1 and CTEQ6M [21] parton distribution functions (PDFs) are used for samples simulated at LO and NLO, respectively. A top quark mass $m_t = 172.5$ GeV is used in the simulation. The response of the full CMS detector is simulated with GEANT4 v9.4 [22, 23], followed by a detailed trigger simulation and event reconstruction. The PYTHIA event generator is used to simulate the presence of additional pp interactions in the same and nearby bunch crossings (“pileup”). Simulated events are reweighted to correct for differences between the number of pileup interactions observed from data and the number produced in the simulation.

A cross section of 244.9 ± 1.4 (stat) $_{-5.5}^{+6.3}$ (syst) ± 6.4 (lumi) pb is used to normalize the $t\bar{t}$ background [24]. The next-to-next-to-leading-order (NNLO) SM prediction is calculated with FEWZ v3.1 [25, 26] for the V +jets backgrounds. The $W+\gamma$ and $Z+\gamma$ simulations are normalized to their

NLO predictions, calculated with MCFM v6.6 [27]. Values of 553.9 pb for the leptonic decay of the $W+\gamma$ process and 159.1 pb for the leptonic decay of the $Z+\gamma$ process are used. The single top quark samples are normalized to their approximate NNLO predictions [28, 29].

4 Event reconstruction and selection

The final state of the signal process in the semileptonic decay channel consists of a high- p_T charged lepton, momentum imbalance due to the presence of a neutrino, jets originating from both the b quarks and from the decay of a W boson, and an energetic photon. Events with either a high- p_T electron or muon are initially selected through a single-lepton trigger. Events in the e +jets final state must pass a trigger requiring an electron with $p_T > 27$ GeV within $|\eta| < 2.5$ and a relative isolation of less than 0.2, where the relative isolation is defined as the sum of the p_T of all particles, excluding the lepton, within a cone around the lepton of $\Delta R = 0.3$, divided by the p_T of the lepton. The μ +jets final state requires a single-muon trigger selecting a muon with $p_T > 24$ GeV within $|\eta| < 2.1$ and relative isolation less than 0.3 within $\Delta R = 0.4$. Events are additionally required to have a well reconstructed primary vertex [30], chosen as the one having the largest sum p_T^2 of the tracks associated with it.

The particle-flow (PF) algorithm is used to reconstruct individual particles in the event [31]. The PF objects include electrons, muons, charged and neutral hadrons, photons, and an imbalance of the transverse momentum. The following describes the selection of reconstructed objects that are used in the analysis.

Electrons are reconstructed from energy deposits in the ECAL matched to a track from the tracker [32]. Electrons are required to have $p_T > 35$ GeV and $|\eta| < 2.5$, excluding the transition region between the barrel and endcap of the ECAL, $1.44 < |\eta| < 1.57$. Electrons from the decay of the top quark are expected to be isolated from other activity in the detector and thus have a requirement that the relative isolation must be less than 0.1. Selected electrons are required to be originating from the primary vertex, and are rejected if identified as likely having originated from a converted photon. Additionally, a multivariate-based identification is applied to reduce the contribution from nonprompt or misidentified electrons. Electrons that fail the above criteria, but pass looser identification requirements ($p_T > 20$ GeV, $|\eta| < 2.5$, and a relative isolation less than 0.2 within a cone of size $\Delta R = 0.3$) are considered to be “loose” electrons. The presence of loose electrons can then be used to reject events from the dilepton final state.

Muons are reconstructed based on measurements from both the tracker and muon systems. Selected muons are required to have $p_T > 26$ GeV and $|\eta| < 2.1$. A requirement on relative isolation less than 0.2 within a cone of $\Delta R = 0.4$ is applied. Loose muons are defined as failing the tight requirements but passing a selection in which the p_T threshold is lowered to 10 GeV and $|\eta| < 2.5$, with the same requirement on the relative isolation as the tight selection.

Jets are reconstructed from PF candidates clustered using the anti- k_T algorithm with a distance parameter of 0.5 [33, 34]. Jets must have $p_T > 30$ GeV and $|\eta| < 2.4$. To remove the contribution to the jet energy from pileup interaction, charged hadrons candidates associated with other vertices are not included in the clustering, and an offset correction to the energy is applied for the contribution of neutral hadrons that would fall within the jet area. Additionally, corrections for the jet energy scale and resolution are applied in simulation, to account for imperfect measurements of the energy of the jet in the detector [35].

Jets are identified as originating from the hadronization of b quarks (b tagged) using the com-

binned secondary vertex algorithm, which combines secondary vertex and track-based lifetime information to provide a discriminant between jets originating from the fragmentation of b quarks and light quarks or gluons. The b tagging algorithm has an efficiency of approximately 70%, while having a probability of incorrectly b tagging a light jet of only 1.4% [36, 37].

Photons are reconstructed as energy deposits in the ECAL that are not matched to track seeds in the pixel detector [12]. The photon is required to have $p_T > 25$ GeV and $|\eta| < 1.44$ (ECAL barrel). A selection based on the shape of the shower caused by the photon in the ECAL is applied using the $\sigma_{\eta\eta}$ variable, which measures the lateral spread of energy in the η space [12]. Selected photons are required to have $\sigma_{\eta\eta} < 0.012$. This is used to distinguish genuine photons from hadronic activity that can be reconstructed as a photon, as the latter will tend to produce a wider energy spread in η , leading to a larger value of $\sigma_{\eta\eta}$. As photons can convert into a pair of electrons before reaching the calorimeter, photon showers along ϕ can be larger compared to that of an electron. Thus, the isolation is defined differently for photons than it was for leptons, in order to account for a possible energy leakage along ϕ . A characteristic photon energy deposition profile, or “footprint”, is used to restrict the area used to calculate isolation of the photon candidate. The charged-hadron isolation variable for photons is defined as the sum of the p_T of all charged hadrons spatially separated from the photon candidate by $\Delta R = 0.3$, but not falling within the photon footprint. The charged-hadron isolation is required not to exceed 5 GeV for selected photons, to help distinguish prompt photons from nonprompt photons produced from hadronic activity.

The missing transverse momentum (p_T^{miss}) is defined as the magnitude of the vector sum of the momenta of all reconstructed PF candidates in the event, projected on the plane perpendicular to the beams.

The final event selection is divided in two steps: a preselection designed to select events with the same topology as top quark pairs (referred to as the “top quark selection”), and a “photon selection”. The top quark selection requires:

- exactly one lepton passing the selection requirements (either an electron or muon);
- no other lepton candidates passing loose selection criteria;
- at least 3 jets, with at least one of these jets passing the b tagging requirement; and
- $p_T^{\text{miss}} > 20$ GeV.

The photon selection requires that events pass the top quark selection and additionally have at least one photon passing the identification and isolation requirements described above.

5 Analysis strategy

After the photon selection is applied, over half of the events in simulation originate from background processes, and not $t\bar{t}+\gamma$ production. The two largest backgrounds are from $t\bar{t}$ events that have a nonprompt photon coming from jets in the event and from $V+\gamma$ events. There is not a single variable that can sufficiently discriminate both of these backgrounds from the $t\bar{t}+\gamma$ signal. The $V+\gamma$ background can be differentiated from $t\bar{t}+\gamma$ events by attempting to reconstruct a top quark in the event. However, $t\bar{t}$ events are very similar to the signal in this respect. Alternatively, the nonprompt photon from the $t\bar{t}$ background will tend to be less isolated than the photons from the $t\bar{t}+\gamma$ signal, but the photon isolation variable does not have discrimination power to distinguish the $V+\gamma$ background from $t\bar{t}+\gamma$ events. In order to be able to distinguish both $t\bar{t}$ and $V+\gamma$ background events, both of these methods are used and the results are combined to measure the $t\bar{t}+\gamma$ yield observed in data.

The fraction of events passing the photon selection containing top quark pairs, referred to as the “top quark purity”, can be measured by reconstructing the hadronically decaying top quark in the event. The M_3 variable, defined as the invariant mass of the three-jet combination that gives the highest vector sum of individual jet transverse momenta, is used for this purpose. Section 7 describes the fit to the distribution of the M_3 variable, used to distinguish top quark pair events from other backgrounds.

Section 8 describes the measurement of the “photon purity”, defined as the fraction of reconstructed photons in the selection region, which come from genuine, isolated photons as opposed to misidentified photons originating from jets. A fit to the photon isolation is used to measure this quantity, which can discriminate between the genuine photons expected from signal and the nonprompt photons from the $t\bar{t}$ background.

The fits for extracting the top quark and photon purity are performed sequentially, and then the values are used in a likelihood function, from which a fit is performed to extract the number of events that originate from the $t\bar{t}+\gamma$ signal process. The likelihood fit and extraction of the number of $t\bar{t}+\gamma$ events are described in Section 9.

6 Multijet and Z+jets background estimation

The quantum chromodynamics (QCD) multijet process is not adequately modeled by simulation, so a data-based approach is applied to measure the shape and normalization of this background component. The shape of the QCD multijet background is taken from a sideband region in data. The sideband region is defined by inverting the lepton relative isolation requirement, selecting leptons with a relative isolation greater than 0.25. Additionally, in the e+jets final state the requirement on the multivariate-based electron identification is inverted, selecting electrons that would typically be identified as misidentified or nonprompt. This control region is dominated by QCD multijet events, with only minor contributions from other processes such as $t\bar{t}$ and W+jets. The small contribution in the control region from other processes is subtracted using simulation to provide shapes of the variable distributions used in the analysis.

The normalization of the QCD multijet background is measured through a binned maximum-likelihood fit to the p_T^{miss} distribution after the standard top quark selection is applied. The distribution of p_T^{miss} is softer in the QCD multijet background than the other processes considered, and thus provides some discriminating power for this background. For the purposes of the fit, the selection requirement on p_T^{miss} is removed, in order to improve the discriminating power of the fit by bringing in more multijet events into the fit region. Two distributions are used in the fit, one for the multijet background and one for the contribution from all other processes. The distribution for the multijet background is taken from the shape found in the sideband control region, while the second distribution is taken from the sum of all simulated events (which does not include the QCD background component). The fit is performed separately in the e+jets and μ +jets final states, and the results are used to scale the QCD multijet background distributions later in the analysis.

The normalization and modeling of the Z+jets background distribution is taken from simulation, but the normalization is corrected by applying a scale factor derived from a fit to data. In order to check the normalization, the selection is modified, selecting same-flavor dilepton events, while keeping all other top quark selection requirements in place. A binned maximum-likelihood fit is performed to the dilepton invariant mass for events passing this modified selection. The fit is performed using two normalized distributions (templates) from simulation,

a Z+jets template and a background template, which predominantly contains $t\bar{t}$ events. Scale factors for the normalization of the Z+jets background are derived from the fit and applied to the simulation.

7 Estimate of top quark pair production

The number of events containing top quark pairs, both after the top quark selection and for events passing the photon selection, are extracted through a binned maximum-likelihood fit to the distribution of the M_3 variable. In events with semileptonic decays of the top quark pair, the M_3 variable provides a simple reconstruction of the hadronically decaying top quark, and has a distribution peaking at the mass of the top quark. Other processes have a wider M_3 distribution.

Two separate fits are performed to the M_3 distribution. The first fit is performed after the top quark selection, to extract the total number of $t\bar{t}$ events passing the selection, $N_{t\bar{t}}$. The second fit is performed for events passing the photon selection in order to measure the top quark purity.

7.1 Measurement of the $t\bar{t}$ yield

The fit to the M_3 distribution for events passing the top quark selection is used to extract the total number of top quark pairs, used for measuring the $t\bar{t}$ component of the cross section ratio. The fit uses three templates: associated to top quark events (taken from $t\bar{t}$ and $t\bar{t}+\gamma$ simulation), W+jets, and other background processes. The template for the other background processes is a combination of the data-based QCD multijet background and all other simulated samples. In the fit, the normalizations of the top quark and W+jets templates are allowed to float, while the normalizations of the other backgrounds templates are kept fixed. The QCD multijet background is normalized to the fit to the p_T^{miss} distribution, while other simulated samples are scaled to their theoretical cross sections. From the fit, 162168 ± 1565 (stat) and 219128 ± 1869 (stat) $t\bar{t}$ events are observed in the e+jets and μ +jets final states, respectively, consistent with the expected total number of $t\bar{t}$ events. The fit results are used to scale the normalization of the $t\bar{t}$ and W+jets contributions in the rest of the analysis.

7.2 Measurement of the top quark purity

After the photon selection, a fit to the M_3 distribution is used to measure the top quark purity. The fit uses three templates: associated to top quark events, W+ γ events, and the sum of all other processes. In the fit, the normalizations of the top quark and W+ γ templates are varied, while the templates of all other processes remain fixed. The top quark template contains simulated events for both $t\bar{t}+\gamma$ and $t\bar{t}$ samples. Figure 2 shows the normalized M_3 distributions for $t\bar{t}+\gamma$, $t\bar{t}$, W+ γ , and other background processes. The backgrounds from non-top quark processes have a wider distribution in this variable, while the $t\bar{t}+\gamma$ and $t\bar{t}$ processes peak near the top quark mass with a tail caused by events with an incorrect assignment of the jets. The relative contributions of the $t\bar{t}+\gamma$ and $t\bar{t}$ samples to the top quark template are computed from the expected yields from simulation, though this does not change the shape of the top quark template as the two distributions are compatible. After the photon selection is applied, the distribution of the M_3 variable in many of the background processes begins to suffer from fluctuations caused by the limited number of simulated events. Because the photon selection does not change the shape of the M_3 distribution, the problem is solved by taking the shapes for the non- $t\bar{t}$ processes from the events after the top quark selection, while retaining the normalization of the samples observed after the photon selection is applied.

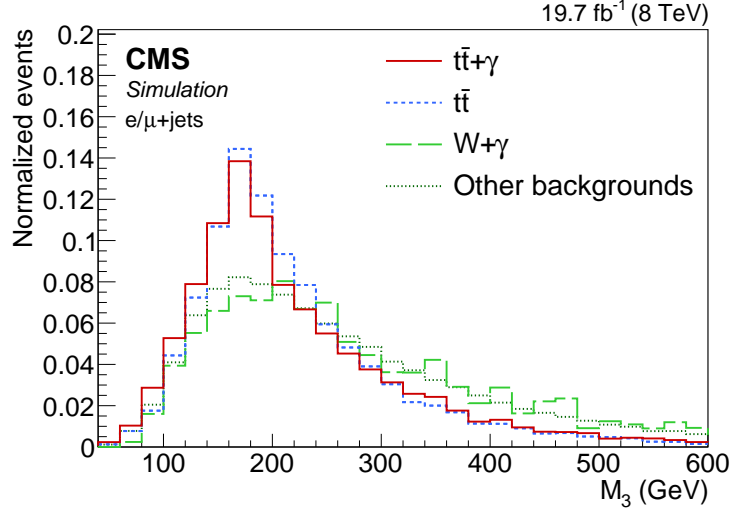


Figure 2: Normalized distributions of the M_3 variable for $t\bar{t}+\gamma$, $t\bar{t}$, $W+\gamma$, and other background processes in a combination of the e +jets and μ +jets final state after the photon selection.

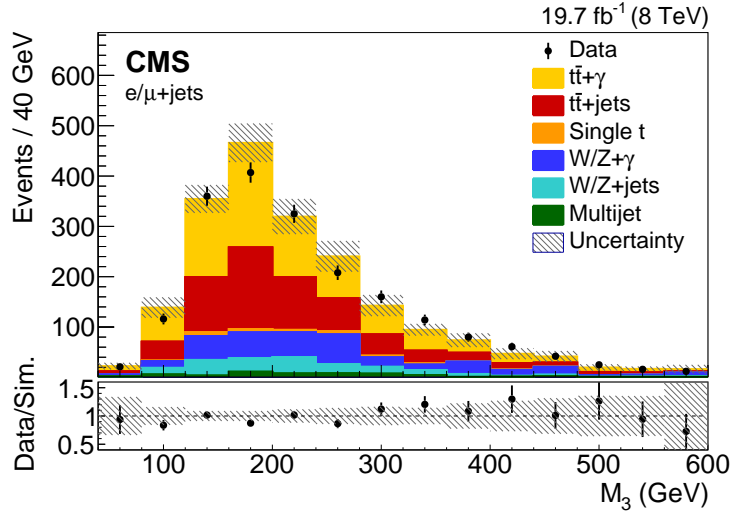


Figure 3: Distribution of the M_3 variable in data and simulation, scaled to the result of the fit in a combination of the e +jets and μ +jets channels, for events passing the photon selection. The lower panel shows the ratio of the data to the prediction from simulation. The uncertainty band is a combination of statistical and systematic uncertainties in the simulation.

Figure 3 shows the distribution of the M_3 variable in data and simulation, scaled to the result of the fit. From the fit result, the top quark purity is measured to be 0.70 ± 0.08 (stat) and 0.68 ± 0.06 (stat) in the e +jets and μ +jets channels, respectively. These are consistent with the expected values from simulation of 0.70 ± 0.03 (stat) in the e +jets final state and 0.72 ± 0.02 (stat) in the μ +jets final state, where the uncertainties are due to the limited number of simulated events.

8 Photon purity measurement

Events are sorted into one of three categories based on the origin of their reconstructed photons. Genuine photons are those which are promptly produced, originating from nonhadronic sources. Misidentified photons can come from misreconstructed electrons, for which the track

from the electron is not correctly reconstructed or properly matched to the energy cluster in the calorimeter, causing the electron to be reconstructed as a photon. Quark or gluon fragmentation and hadronization processes can be misidentified as photons or yield genuine photons, which for both cases are expected to be nonisolated, in contrast with promptly produced photons. The $t\bar{t}+\gamma$ signal events predominantly fall within the first category while the latter two categories are mostly composed of background events.

Simulated events can be placed in one of these three categories based on matching between the reconstructed and generated photons. Matching is performed based on the difference between the reconstructed photon and the generated particles in both p_T and the η - ϕ phase space. If a reconstructed photon is matched to a generated photon from a nonhadronic source, it is classified in the first category. Reconstructed photons that are not matched to a generated photon but instead are matched to a generated electron are classified as misidentified electrons, and placed in the second category. All other events, which are not matched to either a generated photon or electron, are considered to be nonprompt photons originating from hadronic activity and placed in the third category.

Photons in the last category, which are produced from hadronic activity, are typically less isolated than genuine photons or misidentified electrons. This difference in the isolation distribution is used to measure the photon purity, defined as the fraction of events with a photon originating from an isolated source (including both genuine photons and misidentified electrons). A binned maximum-likelihood fit to the distribution of the charged-hadron isolation is used to measure the photon purity.

Templates for the shape of the charged-hadron isolation for isolated photons (coming from either genuine photons or misidentified electrons) and nonprompt (nonisolated) photons are taken from data. The shape of the charged-hadron isolation for the isolated photon template is obtained using the random cone isolation method [38]. In this method, the sum of the transverse energy of PF charged-hadron candidates is measured within a cone of size $\Delta R = 0.3$ at the same η value as the reconstructed photon, but in a random ϕ direction. Contributions to the isolation sum from charged hadrons coming from pileup interactions are subtracted from the energy in the cone. This gives an estimate of the isolation of a completely isolated particle. The shape of the charged-hadron isolation for nonprompt photon events is taken from a sideband region. The charged-hadron isolation of events with a photon having $\sigma_{\eta\eta}$ between 0.012 and 0.016 is used to construct the template for nonisolated photons. These events typically have nonprompt, hadronically produced photons. Comparisons of the distributions of the charged-hadron isolation templates for isolated and nonprompt photons extracted from the data-based method and the templates taken from simulation using the generated particle matching are shown in Fig. 4.

In order to reduce the statistical fluctuations in the background template, the selection requirement of the photon charged-hadron isolation being less than 5 GeV is relaxed during the fit. Instead, the fit is performed in the range of charged-hadron isolation less than 20 GeV, with all other photon selection requirements still in place. The distribution suffers from lower statistical precision at higher values of the isolation, so the distribution is rebinned with larger bins for higher isolation values and finer binning for lower values where the statistical precision is better. Figure 5 shows the result of the fit of the photon charged-hadron isolation in a combination of the e +jets and μ +jets final state. The photon purity is measured based on the fraction of events coming from isolated sources after the charged-hadron isolation requirement is put back in place. The photon purity is measured to be 0.57 ± 0.06 (stat) and 0.53 ± 0.06 (stat) in the e +jets and μ +jets final states, respectively. The expected value for the photon purity in simula-

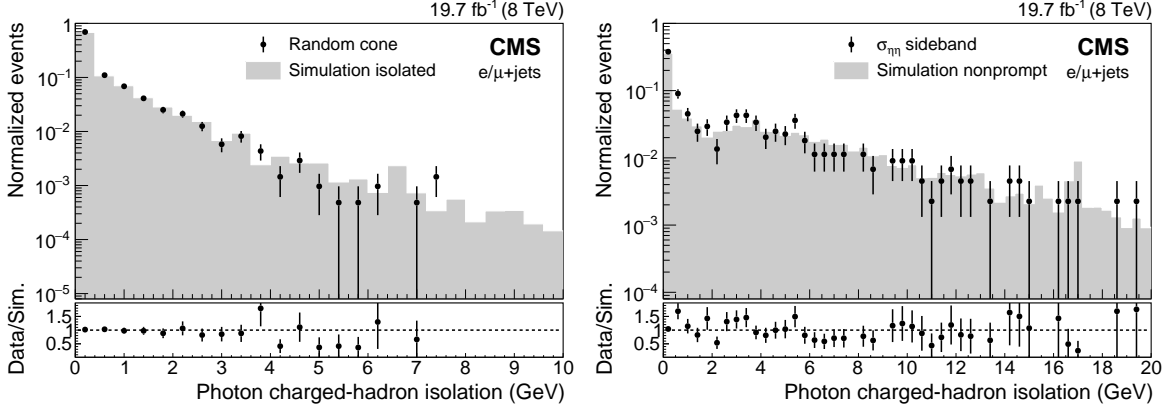


Figure 4: Shapes of isolated (left) and nonprompt (right) photon templates of the photon charged-hadron isolation, comparing templates derived from data to the distributions found from simulation in a combination of the $e+jets$ and $\mu+jets$ final states. The lower panel shows the ratio of the distributions derived from data to those found from simulation.

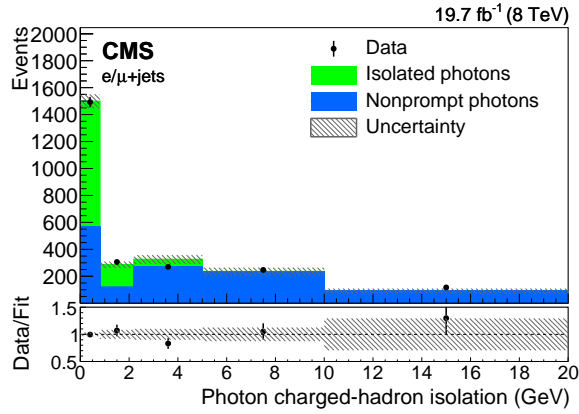


Figure 5: Result of the fit to the photon charged-hadron isolation in a combination of the $e+jets$ and $\mu+jets$ final states. The uncertainty band shows the statistical uncertainties in the templates derived from data. The lower panel shows the ratio of the distribution observed in data to the sum of the templates scaled to the fit result.

tion, assuming the SM prediction for $t\bar{t}+\gamma$ production, is 0.58 ± 0.03 in the $e+jets$ final state and 0.57 ± 0.02 in the $\mu+jets$ final state.

In order to correct the rate of misidentified electrons in simulation, the $Z \rightarrow e^+e^-$ process is used to measure events in which one of the electrons from the Z boson decay is misidentified as a photon. If the photon originates from a misidentified electron from the Z boson decay, the invariant mass of the combination of the electron and photon in the event will be near the Z boson mass.

Under the nominal event selection described previously, the contribution from Z boson production is highly suppressed and does not provide a large enough sample of events to measure the electron misidentification rate accurately. In order to improve the statistical precision, the event selection is modified by relaxing the requirement of having a b -tagged jet in the event, while keeping all other requirements the same. This enhances the contribution of $Z \rightarrow e^+e^-$ events. All steps for the multijet estimation and M_3 fit are repeated for this new selection.

The removal of the b tagging requirement makes the Z boson mass peak much more pro-

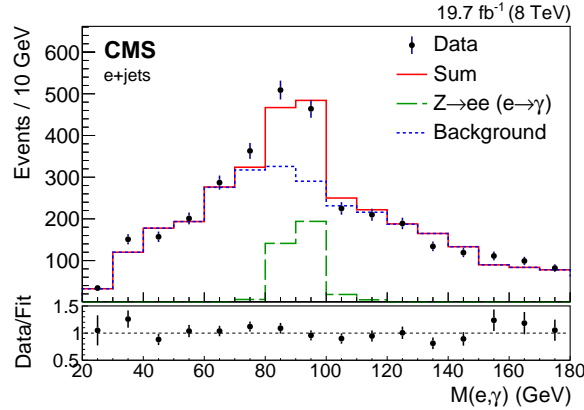


Figure 6: Result of the fit to the invariant mass of the electron and photon for events passing the modified event selection with the b tagging requirement relaxed. Distributions are shown scaled to the results of the fit for $Z \rightarrow ee$ ($e \rightarrow \gamma$) and all other simulated samples (dashed lines), as well as the sum of the two samples (solid line). The lower panel shows the ratio of the data to the simulation scaled to the fit results.

nounced in the $e\gamma$ invariant mass distribution. This allows a template fit to be performed, in order to estimate how well the misidentification of an electron as a photon is modeled in simulation. The fit to the $e\gamma$ invariant mass is performed using two templates, both derived from simulation. The first template consists of events with Z bosons in which the reconstructed photon is matched to one of the electrons from the Z boson decay at the generator level. The second template consists of all other simulated samples not included in the previous template and the data-based multijet sample. The result of the fit is shown in Fig. 6. A scale factor of 1.46 ± 0.20 (stat) is found for simulated events with a misidentified electron. This scale factor is applied to all simulated events in which the photon is identified as originating from a misidentified electron.

9 The $t\bar{t} + \gamma$ yield measurement

Table 1: Simulated samples categorized by reconstructed photon origin, after photon selection in the e +jets channel. The data-based multijet sample is not expected to have signal photons or electrons. All uncertainties combine statistical and systematic contributions.

Sample	Genuine photon	Misid. electron	Nonprompt photon	Total
$t\bar{t} + \gamma$	312 ± 17	0.2 ± 0.1	8.5 ± 0.9	321 ± 17
$t\bar{t}$ +jets	—	22 ± 3	215 ± 13	237 ± 14
$W + \gamma$	75 ± 25	—	—	75 ± 25
W +jets	—	—	60 ± 15	60 ± 15
$Z + \gamma$	14 ± 5	1.3 ± 1.1	$0.5^{+0.7}_{-0.5}$	16 ± 5
Z +jets	—	43 ± 28	11 ± 6	54 ± 30
Single t	11 ± 3	2.0 ± 1.3	16 ± 4	29 ± 7
QCD multijet	—	—	31 ± 18	31 ± 18
Total	412 ± 31	69 ± 29	342 ± 28	823 ± 52
Data	—	—	—	935

As previously mentioned, reconstructed photons originate from either a genuine photon, a misidentified electron, or a jet that produces a nonprompt photon. Different processes contribute to each of these three categories in different ways. For example, the $t\bar{t} + \gamma$ and $V + \gamma$ pro-

Table 2: Simulated samples categorized by reconstructed photon origin, after photon selection in the μ +jets channel. The data-based multijet sample is not expected to have signal photons or electrons. All uncertainties combine statistical and systematic contributions.

Sample	Genuine photon	Misid. electron	Nonprompt photon	Total
$t\bar{t}+\gamma$	407 ± 23	0.4 ± 0.3	11 ± 1	418 ± 24
$t\bar{t}$ +jets	—	31 ± 5	291 ± 16	322 ± 17
$W+\gamma$	140 ± 41	—	9.0 ± 6.7	149 ± 45
W +jets	—	—	57 ± 14	57 ± 14
$Z+\gamma$	21 ± 7	—	1.4 ± 0.9	23 ± 7
Z +jets	—	—	9.6 ± 5.8	10 ± 6
Single t	12 ± 3	1.5 ± 1.3	25 ± 13	38 ± 14
QCD multijet	—	—	36 ± 20	36 ± 20
Total	580 ± 48	33 ± 5	440 ± 33	1053 ± 61
Data	—	—	—	1136

cesses predominantly produce genuine photons, while the $t\bar{t}$ and V +jets processes contribute to the nonprompt-photon or misidentified-electrons categories. The breakdown of the number of events in the three reconstructed photon categories from each of the different simulated processes as well as the total number of expected and observed events are shown in Tables 1 and 2 for the e +jets and μ +jets final states, respectively.

The modeling of misidentified electrons has been corrected using the scale factor described in Section 8, but the modeling of nonprompt photons from jets remains uncorrected. The normalization of the $t\bar{t}$ +jets, W +jets, Z +jets, and QCD samples have been cross-checked and corrected as described previously in Sections 6 and 7. The contribution from single top quark processes is expected to be small and accurately modeled, and is left normalized to the theoretical cross sections. This leaves three major contributing sources, which have so far not been constrained and for which scale factors still need to be measured: $t\bar{t}+\gamma$, $V+\gamma$, and photons originating from jets.

The three remaining scale factors, the scale factor on $t\bar{t}+\gamma$ simulation ($SF_{t\bar{t}+\gamma}$), on $V+\gamma$ simulation ($SF_{V+\gamma}$), and on simulation of photons originating from jets ($SF_{\text{jet}\rightarrow\gamma}$), are derived by defining a likelihood function based on the three previously measured quantities: the photon purity, $\pi_{e\gamma}^{\text{data}}$; top quark purity, $\pi_{t\bar{t}}^{\text{data}}$; and the number of events in data after the photon selection, N^{data} . The likelihood function is defined as $\mathcal{L}(SF_{t\bar{t}+\gamma}, SF_{V+\gamma}, SF_{\text{jet}\rightarrow\gamma}) = e^{-\chi^2/2}$ where χ^2 is the sum of three terms:

$$\chi^2(SF_{t\bar{t}+\gamma}, SF_{V+\gamma}, SF_{\text{jet}\rightarrow\gamma}) = \frac{(\pi_{e\gamma}^{\text{data}} - \pi_{e\gamma}^{\text{MC}})^2}{\sigma_{\pi_{e\gamma}}^2} + \frac{(\pi_{t\bar{t}}^{\text{data}} - \pi_{t\bar{t}}^{\text{MC}})^2}{\sigma_{\pi_{t\bar{t}}}^2} + \frac{(N^{\text{data}} - N^{\text{MC}})^2}{\sigma_N^2}, \quad (1)$$

where $\pi_{e\gamma}^{\text{MC}}$, $\pi_{t\bar{t}}^{\text{MC}}$, and N^{MC} are the photon purity, top quark purity, and the number of events expected from simulation, and $\sigma_{\pi_{e\gamma}}$, $\sigma_{\pi_{t\bar{t}}}$, and σ_N are the statistical uncertainties in the measured quantities. The value of the photon purity from simulation is taken to be the fraction of events in which the reconstructed photon originates from either a genuine photon or a misidentified electron. Similarly, the top quark purity in simulation is found as the fraction of the total simulated events coming from either the $t\bar{t}$ or $t\bar{t}+\gamma$ processes. Because these three values depend on the relative contribution of events from the different processes, they are functions of the three scale factors, $SF_{t\bar{t}+\gamma}$, $SF_{V+\gamma}$, and $SF_{\text{jet}\rightarrow\gamma}$. For example, the photon purity would be increased for larger values of $SF_{t\bar{t}+\gamma}$ or $SF_{V+\gamma}$ whereas $SF_{\text{jet}\rightarrow\gamma}$ would increase the number of nonprompt photons and have the inverse effect on the photon purity. Similarly the top quark purity would be increased for larger values of $SF_{t\bar{t}+\gamma}$ or $SF_{\text{jet}\rightarrow\gamma}$ (since $t\bar{t}$ is the largest contributor of nonprompt

photons), whereas $SF_{V+\gamma}$ has the inverse effect. The likelihood fit is performed by scanning over the possible combinations of the three scale factors to find the one that results in values of $\pi_{e\gamma}^{MC}$, $\pi_{\bar{t}\bar{t}}^{MC}$, and N^{MC} , which most closely match the values observed in data, and thus returns the maximum likelihood value.

The likelihood fit is performed in the e+jets and μ +jets final states individually, as well as in a combination of the two channels. The combination is performed by maximizing the product of the likelihood functions from the e+jets and μ +jets final states.

The scale factors obtained in the likelihood fit are applied to the simulation to extract the number of $\bar{t}\bar{t}+\gamma$ events observed, $N_{\bar{t}\bar{t}+\gamma}$. All $\bar{t}\bar{t}+\gamma$ events are scaled by $SF_{\bar{t}\bar{t}+\gamma}$, and those which fall within the nonprompt-photon category are additionally scaled by $SF_{\text{jet}\rightarrow\gamma}$. Applying the results of the fit in a combination of the e+jets and μ +jets final states, 780 ± 119 (stat) $\bar{t}\bar{t}+\gamma$ events are observed, 338 ± 53 (stat) events and 442 ± 69 (stat) events in the e+jets and μ +jets final states, respectively. The uncertainty comes predominantly from the statistical uncertainty in the results of the likelihood fit.

10 Calculation of the cross section ratio

The fiducial $\bar{t}\bar{t}+\gamma$ cross section ($\sigma_{\bar{t}\bar{t}+\gamma}^{\text{fid.}}$) and the inclusive $\bar{t}\bar{t}+\gamma$ cross section ($\sigma_{\bar{t}\bar{t}+\gamma}$) can be calculated based on the equations:

$$\sigma_{\bar{t}\bar{t}+\gamma}^{\text{fid.}} = \frac{N_{\bar{t}\bar{t}+\gamma}}{\epsilon^{\bar{t}\bar{t}+\gamma} L}, \quad \sigma_{\bar{t}\bar{t}+\gamma} = \frac{N_{\bar{t}\bar{t}+\gamma}}{A^{\bar{t}\bar{t}+\gamma} \epsilon^{\bar{t}\bar{t}+\gamma} L} = \frac{\sigma_{\bar{t}\bar{t}+\gamma}^{\text{fid.}}}{A^{\bar{t}\bar{t}+\gamma}}, \quad (2)$$

where $N_{\bar{t}\bar{t}+\gamma}$ is the number of $\bar{t}\bar{t}+\gamma$ events observed, $A^{\bar{t}\bar{t}+\gamma}$ is the acceptance of $\bar{t}\bar{t}+\gamma$ events within the fiducial phase space, $\epsilon^{\bar{t}\bar{t}+\gamma}$ is the efficiency of the $\bar{t}\bar{t}+\gamma$ selection within events in the acceptance region, and L is the integrated luminosity of the data set.

The acceptance is determined at generator level, by requiring generated events to fall within the fiducial phase space defined for the analysis. Events are required to have exactly one generated prompt lepton in the fiducial phase space. For electrons, this requires $p_T > 35$ GeV and $|\eta| < 2.5$ while not falling in the region $1.44 < |\eta| < 1.56$. The visible phase space for muons is defined as $p_T > 26$ GeV and $|\eta| < 2.5$. Events are required to have at least three generated jets with $p_T > 30$ GeV and $|\eta| < 2.4$. In order to replicate the p_T^{miss} requirement, the vector sum of the p_T of generated neutrinos is required to be greater than 20 GeV. Lastly, events are required to have a generated photon with $p_T > 25$ GeV and $|\eta| < 1.44$. The acceptance can be split into two components: the one coming from the branching fraction of $\bar{t}\bar{t}+\gamma$ to the e+jets or μ +jets channels, and the one coming from the kinematic phase space requirements. The kinematic acceptance is measured by the number of events passing the kinematic phase space requirements described above divided by the number of events generated in the e+jets and μ +jets final states.

The efficiency is calculated as the ratio of reconstructed events that pass the event selection over the number of events generated in the fiducial phase space. This accounts for the migration of events into and out of the fiducial phase space, and includes the efficiencies of the trigger requirement, object identification and reconstruction, and the event selection. The measured values for the acceptance and efficiency of the $\bar{t}\bar{t}+\gamma$ selection in the e+jets and μ +jets channels are given in Table 3.

In order to reduce the effect of systematic uncertainties that similarly affect all $\bar{t}\bar{t}$ +jets production modes, the ratio of the cross section of fiducial $\bar{t}\bar{t}+\gamma$ production to the inclusive $\bar{t}\bar{t}$ produc-

Table 3: Kinematic acceptance and efficiency of the $t\bar{t}+\gamma$ selection in the e+jets and μ +jets final states.

	e+jets	μ +jets
Kinematic acceptance	0.2380 ± 0.0014	0.2551 ± 0.0014
Efficiency	0.1198 ± 0.0071	0.1268 ± 0.0070

tion cross section is calculated as

$$R = \frac{\sigma_{t\bar{t}+\gamma}^{\text{fid}}}{\sigma_{t\bar{t}}} = \frac{N_{t\bar{t}+\gamma}}{N_{t\bar{t}}} \frac{\epsilon_{\text{top}}^{t\bar{t}} A_{\text{top}}^{t\bar{t}}}{\epsilon_{t\bar{t}+\gamma}}, \quad (3)$$

where $N_{t\bar{t}}$ is the number of $t\bar{t}$ events passing the top quark selection, and $\epsilon_{\text{top}}^{t\bar{t}}$ and $A_{\text{top}}^{t\bar{t}}$ are the efficiency and acceptance of top quark selection for $t\bar{t}$ events. The value of $\epsilon_{\text{top}}^{t\bar{t}} A_{\text{top}}^{t\bar{t}}$ is determined from simulation to be 0.034 in the e+jets final state and 0.046 in the μ +jets final state with negligible statistical uncertainties.

11 Sources of systematic uncertainty

The effects of the systematic uncertainties are estimated by varying the simulated samples according to the uncertainty and repeating the measurement. The top quark purity measurement, photon purity measurement, and likelihood fit are repeated for each source of systematic uncertainty and the new value of the cross section ratio is compared to the nominal value. In this way, an estimate of the effect each source of systematic uncertainty has on the final result is found. Table 4 lists the uncertainties in decreasing order of their effect on the cross section ratio, as found through the combination of the e+jets and μ +jets final states.

The statistical uncertainty in the number of signal events found after maximizing the likelihood fit described in Section 9, dominates the determination of the cross section for $t\bar{t}+\gamma$. It includes the uncertainties in the measurement of the photon purity, top quark purity after photon selection, and the statistical uncertainty from the observed number of events in data. The contribution from each of these three portions is estimated individually by performing the likelihood fit in which the uncertainties in these parameters are set to zero one at a time. This effectively fixes the value to the measured value. The change in the $SF_{t\bar{t}+\gamma}$ uncertainty (which is roughly 14% in the standard likelihood fit) can be attributed to the fixed parameter. The uncertainty is dominated by the top quark purity and photon purity uncertainties, which contribute 10% and 9%, respectively. The statistical uncertainty caused by the limited number of events in data is approximately 4.8%.

The uncertainties in the energy of reconstructed objects in the event are taken into account by scaling the energies of reconstructed objects in simulation up and down by the uncertainties in their corrections. The uncertainties in the jet energy scale (JES) and jet energy resolution (JER) [35] are applied to the reconstructed jets and the effect is propagated to the calculation of p_T^{miss} . Similarly the uncertainty due to the photon energy is found by scaling the energy of reconstructed photons up and down by 1%, and the measurement is repeated [12]. The uncertainty due to the lepton energy scale is found by varying the p_T of the electrons and muons in the event by 1% in the e+jets and μ +jets final states, respectively [32, 39].

A 50% uncertainty is assigned to the normalization of the data-based multijet sample derived from the fit to the p_T^{miss} distributions. Additionally, a 20% normalization uncertainty is applied to the backgrounds that are fixed to their theoretical cross sections in the M_3 fit (described in

Section 7). The systematic uncertainty due to the scale factor for Z+jets simulation (described in Section 6) is applied by adjusting the scale factor up and down by its uncertainty.

The uncertainty in the efficiency of the b tagging algorithm is taken into account by varying the b tagging scale factors up and down by their uncertainties [37]. Differences between the distribution of the p_T of the top quarks in data and simulation are taken into account by applying a reweighting based on the p_T of the generated top quarks and treating the difference from the nominal sample as a systematic uncertainty (“top quark p_T reweighting”) [40]. The uncertainty in the pileup correction is found by recalculating the pileup distribution in data with a plus and minus 5% change to the total inelastic proton-proton cross section [41], and using these new distributions to reweight the simulation.

The uncertainty in the factorization and renormalization scales is taken into account by simulating the $t\bar{t}+\gamma$ and $t\bar{t}$ +jets processes with the scales doubled and halved compared to the nominal value of $\mu_F = \mu_R = Q = \sqrt{m_t^2 + \Sigma p_T^2}$ (where the sum is taken over all final state partons). The uncertainty in the matching of partons at ME level to the parton shower (PS) is found by simulating $t\bar{t}+\gamma$ and $t\bar{t}$ +jets processes with the threshold used for matching doubled and halved from the nominal value of 20 GeV. The uncertainty arising from the choice of the top quark mass used in simulation is measured by simulating the samples with a value of m_t varied up and down by 1 GeV from its central value of $m_t = 172.5$ GeV.

Table 4: Uncertainties in the cross section ratio R for the combination of the e+jets and μ +jets final states.

Source	Uncertainty (%)
Statistical likelihood fit	15.5
Top quark mass	7.9
JES	6.9
Fact. and renorm. scale	6.7
ME/PS matching threshold	3.9
Photon energy scale	2.4
JER	2.3
Multijet estimate	2.0
Electron misid. rate	1.3
Z+jets scale factor	0.8
Pileup	0.6
Background normalization	0.6
Top quark p_T reweighting	0.4
b tagging scale factor	0.3
Muon efficiency	0.3
Electron efficiency	0.1
PDFs	0.1
Muon energy scale	0.1
Electron energy scale	0.1
Total	20.7

12 Results

The ratio of the fiducial cross section of $t\bar{t}+\gamma$ to $t\bar{t}$ production is found to be $R = (5.7 \pm 1.8) \times 10^{-4}$ (stat+syst) in the e+jets final state and $R = (4.7 \pm 1.3) \times 10^{-4}$ (stat+syst) in the μ +jets final state. The value of the fiducial $t\bar{t}+\gamma$ cross section can be extracted from the cross section ratio

using the measured $t\bar{t}$ cross section of 244.9 ± 1.4 (stat) $_{-5.5}^{+6.3}$ (syst) ± 6.4 (lumi) pb [24]. Multiplying the cross section ratio by the measured $t\bar{t}$ cross section results in values for the $t\bar{t}+\gamma$ fiducial cross section of 138 ± 45 (stat+syst) fb in the e+jets final state and 115 ± 32 (stat+syst) fb in the μ +jets final state.

The value of the cross section times the branching fraction in the lepton+jets final states can be extrapolated from the fiducial cross section by dividing by the kinematic acceptance. The kinematic acceptances (as given in Section 10) are found to be 0.2380 ± 0.0014 and 0.2551 ± 0.0014 in the e+jets and μ +jets final states. This gives a cross section times branching fraction of $\sigma_{t\bar{t}+\gamma} \mathcal{B} = 582 \pm 187$ fb in the e+jets final state and 453 ± 124 fb in the μ +jets final state. These values are in agreement with theoretical prediction of 592 ± 71 (scales) ± 30 (PDFs) fb for the cross section times branching fraction of each of the semileptonic final states [42].

The combination of the e+jets and μ +jets channels results in a cross section ratio per semileptonic final state of $(5.2 \pm 1.1) \times 10^{-4}$ (stat+syst). This results in a value of 127 ± 27 (stat+syst) fb for the fiducial $t\bar{t}+\gamma$ cross section. When extrapolated to the cross section times branching fraction by dividing by the kinematic acceptance, the result is $\sigma_{t\bar{t}+\gamma} \mathcal{B} = 515 \pm 108$ fb per lepton+jets final state, in good agreement with the theoretical prediction. Table 5 summarizes the measured ratios and cross sections for the e+jets and μ +jets final states as well as the combination.

Table 5: Cross section ratios, as well as fiducial and total cross sections per semileptonic final state.

Category	R	$\sigma_{t\bar{t}+\gamma}^{\text{fid}}$ (fb)	$\sigma_{t\bar{t}+\gamma} \mathcal{B}$ (fb)
e+jets	$(5.7 \pm 1.8) \times 10^{-4}$	138 ± 45	582 ± 187
μ +jets	$(4.7 \pm 1.3) \times 10^{-4}$	115 ± 32	453 ± 124
Combination	$(5.2 \pm 1.1) \times 10^{-4}$	127 ± 27	515 ± 108
Theory	—	—	592 ± 71 (scales) ± 30 (PDFs)

The distributions of the transverse momentum and absolute value of the pseudorapidity of the photon candidate are shown in Figs. 7 and 8, scaled to the results of the likelihood fit. While the statistical precision of this analysis currently limits the ability to perform a differential measurement of the $t\bar{t}+\gamma$ cross section, there is the potential to measure the differential cross section in the future in both of these variables.

13 Summary

The results of a measurement of the production of a top quark-antiquark ($t\bar{t}$) pair produced in association with a photon have been presented. The measurement is performed using 19.7 fb^{-1} of data collected by the CMS detector at a center-of-mass energy of 8 TeV. The analysis has been performed in the semileptonic e+jets and μ +jets decay channels.

The ratio of the $t\bar{t}+\gamma$ to $t\bar{t}$ production cross sections has been measured to be $R = \sigma_{t\bar{t}+\gamma}/\sigma_{t\bar{t}} = (5.2 \pm 1.1) \times 10^{-4}$. By multiplying the measured ratio by the previously measured value of the $t\bar{t}$ cross section, the fiducial cross section for $t\bar{t}+\gamma$ production of 127 ± 27 fb has been found for events in the e+jets and μ +jets final states. The measured values are in agreement with the theoretical predictions.

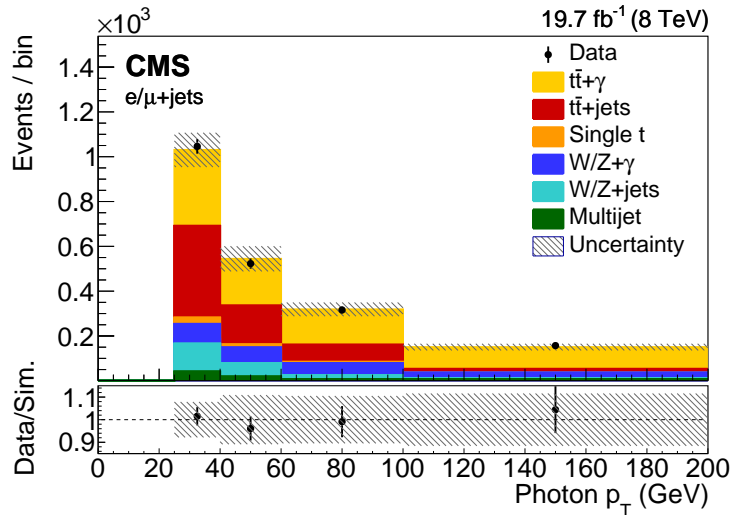


Figure 7: Distribution of the transverse momentum of the photon in data and simulation, scaled to the result of the likelihood fit in a combination of the $e+\text{jets}$ and $\mu+\text{jets}$ channels for events passing the photon selection. The lower panel shows the ratio of the data to the prediction from simulation. The uncertainty band is a combination of statistical and systematic uncertainties in the simulation.

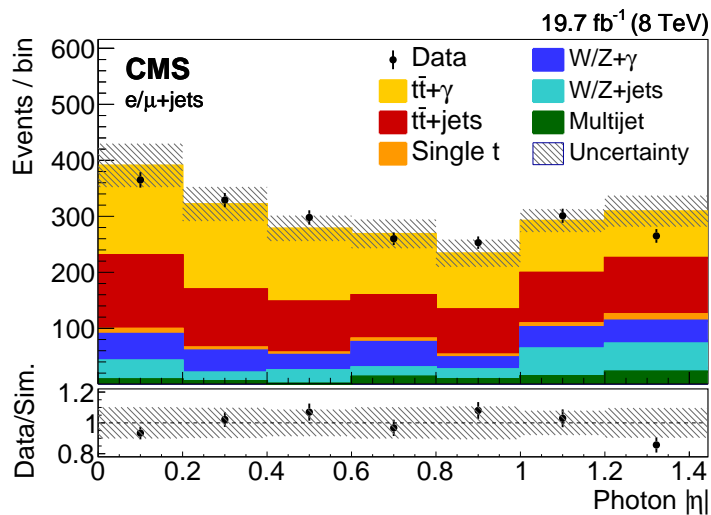


Figure 8: Distribution of the absolute value of the pseudorapidity of the photon in data and simulation, scaled to the result of the likelihood fit in a combination of the $e+\text{jets}$ and $\mu+\text{jets}$ channels for events passing the photon selection. The lower panel shows the ratio of the data to the prediction from simulation. The uncertainty band is a combination of statistical and systematic uncertainties in the simulation.

Acknowledgments

We congratulate our colleagues in the CERN accelerator departments for the excellent performance of the LHC and thank the technical and administrative staffs at CERN and at other CMS institutes for their contributions to the success of the CMS effort. In addition, we gratefully acknowledge the computing centres and personnel of the Worldwide LHC Computing Grid for delivering so effectively the computing infrastructure essential to our analyses. Finally, we acknowledge the enduring support for the construction and operation of the LHC and the CMS detector provided by the following funding agencies: BMWFW and FWF (Austria); FNRS and FWO (Belgium); CNPq, CAPES, FAPERJ, and FAPESP (Brazil); MES (Bulgaria); CERN; CAS, MoST, and NSFC (China); COLCIENCIAS (Colombia); MSES and CSF (Croatia); RPF (Cyprus); SENESCYT (Ecuador); MoER, ERC IUT, and ERDF (Estonia); Academy of Finland, MEC, and HIP (Finland); CEA and CNRS/IN2P3 (France); BMBF, DFG, and HGF (Germany); GSRT (Greece); OTKA and NIH (Hungary); DAE and DST (India); IPM (Iran); SFI (Ireland); INFN (Italy); MSIP and NRF (Republic of Korea); LAS (Lithuania); MOE and UM (Malaysia); BUAP, CINVESTAV, CONACYT, LNS, SEP, and UASLP-FAI (Mexico); MBIE (New Zealand); PAEC (Pakistan); MSHE and NSC (Poland); FCT (Portugal); JINR (Dubna); MON, RosAtom, RAS, RFBR and RAEP (Russia); MESTD (Serbia); SEIDI, CPAN, PCTI and FEDER (Spain); Swiss Funding Agencies (Switzerland); MST (Taipei); ThEPCenter, IPST, STAR, and NSTDA (Thailand); TUBITAK and TAEK (Turkey); NASU and SFFR (Ukraine); STFC (United Kingdom); DOE and NSF (USA).

Individuals have received support from the Marie-Curie programme and the European Research Council and Horizon 2020 Grant, contract No. 675440 (European Union); the Leventis Foundation; the A. P. Sloan Foundation; the Alexander von Humboldt Foundation; the Belgian Federal Science Policy Office; the Fonds pour la Formation à la Recherche dans l'Industrie et dans l'Agriculture (FRIA-Belgium); the Agentschap voor Innovatie door Wetenschap en Technologie (IWT-Belgium); the Ministry of Education, Youth and Sports (MEYS) of the Czech Republic; the Council of Science and Industrial Research, India; the HOMING PLUS programme of the Foundation for Polish Science, cofinanced from European Union, Regional Development Fund, the Mobility Plus programme of the Ministry of Science and Higher Education, the National Science Center (Poland), contracts Harmonia 2014/14/M/ST2/00428, Opus 2014/13/B/ST2/02543, 2014/15/B/ST2/03998, and 2015/19/B/ST2/02861, Sonata-bis 2012/07/E/ST2/01406; the National Priorities Research Program by Qatar National Research Fund; the Programa Clarín-COFUND del Principado de Asturias; the Thalís and Aristeia programmes cofinanced by EU-ESF and the Greek NSRF; the Rachadapisek Sompot Fund for Postdoctoral Fellowship, Chulalongkorn University and the Chulalongkorn Academic into Its 2nd Century Project Advancement Project (Thailand); and the Welch Foundation, contract C-1845.

References

- [1] T. Han, "The 'Top Priority' at the LHC", *Int. J. Mod. Phys. A* **23** (2008) 4107, doi:10.1142/S0217751X08042705, arXiv:0804.3178.
- [2] W. Bernreuther, "Top quark physics at the LHC", *J. Phys. G* **35** (2008) 083001, doi:10.1088/0954-3899/35/8/083001, arXiv:0805.1333.
- [3] A. Buckley et al., "Constraining top quark effective theory in the LHC Run II era", *JHEP* **04** (2016) 015, doi:10.1007/JHEP04(2016)015, arXiv:1512.03360.

- [4] U. Baur, A. Juste, L. H. Orr, and D. Rainwater, "Probing electroweak top quark couplings at hadron colliders", *Phys. Rev. D* **71** (2005) 054013, doi:10.1103/PhysRevD.71.054013.
- [5] A. O. Bouzas and F. Larios, "Electromagnetic dipole moments of the top quark", *Phys. Rev. D* **87** (2013) 074015, doi:10.1103/PhysRevD.87.074015.
- [6] O. Bessidskaia Bylund et al., "Probing top quark neutral couplings in the Standard Model Effective Field Theory at NLO in QCD", *JHEP* **05** (2016) 052, doi:10.1007/JHEP05(2016)052, arXiv:1601.08193.
- [7] M. Schulze and Y. Soreq, "Pinning down electroweak dipole operators of the top quark", *Eur. Phys. J. C* **76** (2016) 466, doi:10.1140/epjc/s10052-016-4263-x, arXiv:1603.08911.
- [8] CDF Collaboration, "Evidence for $t\bar{t}\gamma$ production and measurement of $\sigma_{t\bar{t}\gamma}/\sigma_{t\bar{t}}$ ", *Phys. Rev. D* **48** (2011) 031104, doi:10.1103/PhysRevD.84.031104, arXiv:1106.3970.
- [9] ATLAS Collaboration, "Observation of top-quark pair production in association with a photon and measurement of the $t\bar{t}\gamma$ production cross section in pp collisions at $\sqrt{s} = 7$ TeV using the ATLAS detector", *Phys. Rev. D* **91** (2015) 072007, doi:10.1103/PhysRevD.91.072007, arXiv:1502.00586.
- [10] ATLAS Collaboration, "Measurement of the $t\bar{t}\gamma$ production cross section in proton-proton collisions at $\sqrt{s} = 8$ TeV with the ATLAS detector", (2017). arXiv:1706.03046. Submitted to *JHEP*.
- [11] P.-F. Duan et al., "QCD corrections to associated production of $t\bar{t}\gamma$ at hadron colliders", *Phys. Rev. D* **80** (2009) 014022, doi:10.1103/PhysRevD.80.014022, arXiv:0907.1324.
- [12] CMS Collaboration, "Performance of photon reconstruction and identification with the CMS detector in proton-proton collisions at $\sqrt{s} = 8$ TeV", *JINST* **10** (2015) P08010, doi:10.1088/1748-0221/10/08/P08010, arXiv:1502.02702.
- [13] CMS Collaboration, "The CMS experiment at the CERN LHC", *JINST* **3** (2008) S08004, doi:10.1088/1748-0221/3/08/S08004.
- [14] J. Alwall et al., "The automated computation of tree-level and next-to-leading order differential cross sections, and their matching to parton shower simulations", *JHEP* **07** (2014) 079, doi:10.1007/JHEP07(2014)079, arXiv:1405.0301.
- [15] S. Frixione, P. Nason, and C. Oleari, "Matching NLO QCD computations with parton shower simulations: the POWHEG method", *JHEP* **11** (2007) 070, doi:10.1088/1126-6708/2007/11/070, arXiv:0709.2092.
- [16] S. Alioli, P. Nason, C. Oleari, and E. Re, "A general framework for implementing NLO calculations in shower Monte Carlo programs: the POWHEG BOX", *JHEP* **06** (2010) 043, doi:10.1007/JHEP06(2010)043, arXiv:1002.2581.
- [17] E. Re, "Single-top Wt -channel production matched with parton showers using the POWHEG method", *Eur. Phys. J. C* **71** (2011) 1547, doi:10.1140/epjc/s10052-011-1547-z, arXiv:1009.2450.

- [18] S. Alioli, P. Nason, C. Oleari, and E. Re, “NLO single-top production matched with shower in POWHEG: s - and t -channel contributions”, *JHEP* **09** (2009) 111, doi:10.1088/1126-6708/2009/09/111, arXiv:0907.4076. [Erratum: doi:10.1007/JHEP02(2010)011].
- [19] T. Sjöstrand, S. Mrenna, and P. Skands, “PYTHIA 6.4 physics and manual”, *JHEP* **05** (2006) 026, doi:10.1088/1126-6708/2006/05/026, arXiv:hep-ph/0603175.
- [20] Z. Was, “Precision simulations with TAUOLA and PHOTOS”, *Nucl. Phys. Proc. Suppl.* **169** (2007) 16, doi:10.1016/j.nuclphysbps.2007.02.113, arXiv:hep-ph/0610386.
- [21] P. M. Nadolsky et al., “Implications of CTEQ global analysis for collider observables”, *Phys. Rev. D* **78** (2008) 013004, doi:10.1103/PhysRevD.78.013004, arXiv:0802.0007.
- [22] GEANT4 Collaboration, “GEANT4—a simulation toolkit”, *Nucl. Instrum. Meth. A* **506** (2003) 250, doi:10.1016/S0168-9002(03)01368-8.
- [23] J. Allison et al., “GEANT4 developments and applications”, *IEEE Trans. Nucl. Sci.* **53** (2006) 270, doi:10.1109/TNS.2006.869826.
- [24] CMS Collaboration, “Measurement of the $t\bar{t}$ production cross section in the $e\text{-}\mu$ channel in proton-proton collisions at $\sqrt{s} = 7$ and 8 TeV”, *JHEP* **08** (2016) 029, doi:10.1007/JHEP08(2016)029, arXiv:1603.02303.
- [25] K. Melnikov and F. Petriello, “Electroweak gauge boson production at hadron colliders through $O(\alpha^2)$ ”, *Phys. Rev. D* **74** (2006) 114017, doi:10.1103/PhysRevD.74.114017, arXiv:hep-ph/0609070.
- [26] K. Melnikov and F. Petriello, “W boson production cross section at the Large Hadron Collider with $O(\alpha^2)$ corrections”, *Phys. Rev. Lett.* **96** (2006) 231803, doi:10.1103/PhysRevLett.96.231803, arXiv:hep-ph/0603182.
- [27] J. M. Campbell and R. K. Ellis, “MCFM for the Tevatron and the LHC”, in *Proceedings, 10th DESY Workshop on Elementary Particle Theory: Loops and Legs in Quantum Field Theory*, volume 205-206, p. 10. Woerlitz, Germany, April, 2010. arXiv:1007.3492. *Nucl. Phys. Proc. Suppl.* 205-206 (2010) 10. doi:10.1016/j.nuclphysbps.2010.08.011.
- [28] N. Kidonakis, “Next-to-next-to-leading logarithm resummation for s -channel single top quark production”, *Phys. Rev. D* **81** (2010) 054028, doi:10.1103/PhysRevD.81.054028, arXiv:1001.5034.
- [29] N. Kidonakis, “Two-loop soft anomalous dimensions for single top quark associated production with a W^- or H^- ”, *Phys. Rev. D* **82** (2010) 054018, doi:10.1103/PhysRevD.82.054018, arXiv:1005.4451.
- [30] CMS Collaboration, “Description and performance of track and primary-vertex reconstruction with the CMS tracker”, *JINST* **9** (2014) P10009, doi:10.1088/1748-0221/9/10/P10009, arXiv:1405.6569.
- [31] CMS Collaboration, “Particle-flow reconstruction and global event description with the CMS detector”, (2017). arXiv:1706.04965. Submitted to *JINST*.

- [32] CMS Collaboration, "Performance of electron reconstruction and selection with the CMS detector in proton-proton collisions at $\sqrt{s} = 8$ TeV", *JINST* **10** (2015) P06005, doi:10.1088/1748-0221/10/06/P06005, arXiv:1502.02701.
- [33] M. Cacciari, G. P. Salam, and G. Soyez, "The anti- k_t jet clustering algorithm", *JHEP* **04** (2008) 063, doi:10.1088/1126-6708/2008/04/063, arXiv:0802.1189.
- [34] M. Cacciari, G. P. Salam, and G. Soyez, "FastJet user manual", *Eur. Phys. J. C* **72** (2012) 1896, doi:10.1140/epjc/s10052-012-1896-2, arXiv:1111.6097.
- [35] CMS Collaboration, "Determination of jet energy calibration and transverse momentum resolution in CMS", *JINST* **6** (2011) P11002, doi:10.1088/1748-0221/6/11/P11002.
- [36] CMS Collaboration, "Performance of b tagging at $\sqrt{s} = 8$ TeV in multijet, $t\bar{t}$ and boosted topology events", CMS Physics Analysis Summary CMS-PAS-BTV-13-001, 2013.
- [37] CMS Collaboration, "Identification of b-quark jets with the CMS experiment", *JINST* **8** (2013) P04013, doi:10.1088/1748-0221/8/04/P04013, arXiv:1211.4462.
- [38] CMS Collaboration, "Measurement of differential cross sections for the production of a pair of isolated photons in pp collisions at $\sqrt{s} = 7$ TeV", *Eur. Phys. J. C* **74** (2014) 3129, doi:10.1140/epjc/s10052-014-3129-3, arXiv:1405.7225.
- [39] CMS Collaboration, "Performance of CMS muon reconstruction in pp collision events at $\sqrt{s} = 7$ TeV", *JINST* **7** (2012) P10002, doi:10.1088/1748-0221/7/10/P10002, arXiv:1206.4071.
- [40] CMS Collaboration, "Measurement of the differential cross section for top quark pair production in pp collisions at $\sqrt{s} = 8$ TeV", *Eur. Phys. J. C* **75** (2015) 542, doi:10.1140/epjc/s10052-015-3709-x, arXiv:1505.04480.
- [41] CMS Collaboration, "Measurement of the inelastic proton-proton cross section at $\sqrt{s} = 7$ TeV", *Phys. Lett. B* **722** (2013) 5, doi:10.1016/j.physletb.2013.03.024, arXiv:1210.6718.
- [42] K. Melnikov, M. Schulze, and A. Scharf, "QCD corrections to top quark pair production in association with a photon at hadron colliders", *Phys. Rev. D* **83** (2011) 074013, doi:10.1103/PhysRevD.83.074013, arXiv:1102.1967.

A The CMS Collaboration

Yerevan Physics Institute, Yerevan, Armenia

A.M. Sirunyan, A. Tumasyan

Institut für Hochenergiephysik, Wien, Austria

W. Adam, E. Asilar, T. Bergauer, J. Brandstetter, E. Brondolin, M. Dragicevic, J. Erö, M. Flechl, M. Friedl, R. Frühwirth¹, V.M. Ghete, C. Hartl, N. Hörmann, J. Hrubec, M. Jeitler¹, A. König, I. Krätschmer, D. Liko, T. Matsushita, I. Mikulec, D. Rabady, N. Rad, B. Rahbaran, H. Rohringer, J. Schieck¹, J. Strauss, W. Waltenberger, C.-E. Wulz¹

Institute for Nuclear Problems, Minsk, Belarus

O. Dvornikov, V. Makarenko, V. Mossolov, J. Suarez Gonzalez, V. Zykunov

National Centre for Particle and High Energy Physics, Minsk, Belarus

N. Shumeiko

Universiteit Antwerpen, Antwerpen, Belgium

S. Alderweireldt, E.A. De Wolf, X. Janssen, J. Lauwers, M. Van De Klundert, H. Van Haevermaet, P. Van Mechelen, N. Van Remortel, A. Van Spilbeek

Vrije Universiteit Brussel, Brussel, Belgium

S. Abu Zeid, F. Blekman, J. D'Hondt, N. Daci, I. De Bruyn, K. Deroover, S. Lowette, S. Moortgat, L. Moreels, A. Olbrechts, Q. Python, K. Skovpen, S. Tavernier, W. Van Doninck, P. Van Mulders, I. Van Parijs

Université Libre de Bruxelles, Bruxelles, Belgium

H. Brun, B. Clerbaux, G. De Lentdecker, H. Delannoy, G. Fasanella, L. Favart, R. Goldouzian, A. Grebenyuk, G. Karapostoli, T. Lenzi, A. Léonard, J. Luetic, T. Maerschalk, A. Marinov, A. Randle-conde, T. Seva, C. Vander Velde, P. Vanlaer, D. Vannerom, R. Yonamine, F. Zenoni, F. Zhang²

Ghent University, Ghent, Belgium

A. Cimmino, T. Cornelis, D. Dobur, A. Fagot, M. Gul, I. Khvastunov, D. Poyraz, S. Salva, R. Schöfbeck, M. Tytgat, W. Van Driessche, E. Yazgan, N. Zaganidis

Université Catholique de Louvain, Louvain-la-Neuve, Belgium

H. Bakhshiansohi, C. Beluffi³, O. Bondu, S. Brochet, G. Bruno, A. Caudron, S. De Visscher, C. Delaere, M. Delcourt, B. Francois, A. Giammanco, A. Jafari, M. Komm, G. Krintiras, V. Lemaître, A. Magitteri, A. Mertens, M. Musich, K. Piotrkowski, L. Quertenmont, M. Selvaggi, M. Vidal Marono, S. Wertz

Université de Mons, Mons, Belgium

N. Bely

Centro Brasileiro de Pesquisas Físicas, Rio de Janeiro, Brazil

W.L. Aldá Júnior, F.L. Alves, G.A. Alves, L. Brito, C. Hensel, A. Moraes, M.E. Pol, P. Rebello Teles

Universidade do Estado do Rio de Janeiro, Rio de Janeiro, Brazil

E. Belchior Batista Das Chagas, W. Carvalho, J. Chinellato⁴, A. Custódio, E.M. Da Costa, G.G. Da Silveira⁵, D. De Jesus Damiao, C. De Oliveira Martins, S. Fonseca De Souza, L.M. Huertas Guativa, H. Malbouisson, D. Matos Figueiredo, C. Mora Herrera, L. Mundim, H. Nogima, W.L. Prado Da Silva, A. Santoro, A. Sznajder, E.J. Tonelli Manganote⁴, F. Torres Da Silva De Araujo, A. Vilela Pereira

Universidade Estadual Paulista ^a, Universidade Federal do ABC ^b, São Paulo, Brazil

S. Ahuja^a, C.A. Bernardes^a, S. Dogra^a, T.R. Fernandez Perez Tomei^a, E.M. Gregores^b, P.G. Mercadante^b, C.S. Moon^a, S.F. Novaes^a, Sandra S. Padula^a, D. Romero Abad^b, J.C. Ruiz Vargas^a

Institute for Nuclear Research and Nuclear Energy, Sofia, Bulgaria

A. Aleksandrov, R. Hadjiiska, P. Iaydjiev, M. Rodozov, S. Stoykova, G. Sultanov, M. Vutova

University of Sofia, Sofia, Bulgaria

A. Dimitrov, I. Glushkov, L. Litov, B. Pavlov, P. Petkov

Beihang University, Beijing, China

W. Fang⁶

Institute of High Energy Physics, Beijing, China

M. Ahmad, J.G. Bian, G.M. Chen, H.S. Chen, M. Chen, Y. Chen⁷, T. Cheng, C.H. Jiang, D. Leggat, Z. Liu, F. Romeo, M. Ruan, S.M. Shaheen, A. Spiezia, J. Tao, C. Wang, Z. Wang, H. Zhang, J. Zhao

State Key Laboratory of Nuclear Physics and Technology, Peking University, Beijing, China

Y. Ban, G. Chen, Q. Li, S. Liu, Y. Mao, S.J. Qian, D. Wang, Z. Xu

Universidad de Los Andes, Bogota, Colombia

C. Avila, A. Cabrera, L.F. Chaparro Sierra, C. Florez, J.P. Gomez, C.F. González Hernández, J.D. Ruiz Alvarez, J.C. Sanabria

University of Split, Faculty of Electrical Engineering, Mechanical Engineering and Naval Architecture, Split, Croatia

N. Godinovic, D. Lelas, I. Puljak, P.M. Ribeiro Cipriano, T. Sculac

University of Split, Faculty of Science, Split, Croatia

Z. Antunovic, M. Kovac

Institute Rudjer Boskovic, Zagreb, Croatia

V. Brigljevic, D. Ferencek, K. Kadija, B. Mesic, T. Susa

University of Cyprus, Nicosia, Cyprus

A. Attikis, G. Mavromanolakis, J. Mousa, C. Nicolaou, F. Ptochos, P.A. Razis, H. Rykaczewski, D. Tsiakkouri

Charles University, Prague, Czech Republic

M. Finger⁸, M. Finger Jr.⁸

Universidad San Francisco de Quito, Quito, Ecuador

E. Carrera Jarrin

Academy of Scientific Research and Technology of the Arab Republic of Egypt, Egyptian Network of High Energy Physics, Cairo, Egypt

E. El-khateeb⁹, S. Elgammal¹⁰, A. Mohamed¹¹

National Institute of Chemical Physics and Biophysics, Tallinn, Estonia

M. Kadastik, L. Perrini, M. Raidal, A. Tiko, C. Veelken

Department of Physics, University of Helsinki, Helsinki, Finland

P. Eerola, J. Pekkanen, M. Voutilainen

Helsinki Institute of Physics, Helsinki, Finland

J. Härkönen, T. Järvinen, V. Karimäki, R. Kinnunen, T. Lampén, K. Lassila-Perini, S. Lehti, T. Lindén, P. Luukka, J. Tuominiemi, E. Tuovinen, L. Wendland

Lappeenranta University of Technology, Lappeenranta, Finland

J. Talvitie, T. Tuuva

IRFU, CEA, Université Paris-Saclay, Gif-sur-Yvette, France

M. Besancon, F. Couderc, M. Dejardin, D. Denegri, B. Fabbro, J.L. Faure, C. Favaro, F. Ferri, S. Ganjour, S. Ghosh, A. Givernaud, P. Gras, G. Hamel de Monchenault, P. Jarry, I. Kucher, E. Locci, M. Machet, J. Malcles, J. Rander, A. Rosowsky, M. Titov

Laboratoire Leprince-Ringuet, Ecole polytechnique, CNRS/IN2P3, Université Paris-Saclay, Palaiseau, France

A. Abdulsalam, I. Antropov, S. Baffioni, F. Beaudette, P. Busson, L. Cadamuro, E. Chapon, C. Charlot, O. Davignon, R. Granier de Cassagnac, M. Jo, S. Lisniak, P. Miné, M. Nguyen, C. Ochando, G. Ortona, P. Paganini, P. Pigard, S. Regnard, R. Salerno, Y. Sirois, A.G. Stahl Leiton, T. Strebler, Y. Yilmaz, A. Zabi, A. Zghiche

Université de Strasbourg, CNRS, IPHC UMR 7178, F-67000 Strasbourg, France

J.-L. Agram¹², J. Andrea, A. Aubin, D. Bloch, J.-M. Brom, M. Buttignol, E.C. Chabert, N. Chanon, C. Collard, E. Conte¹², X. Coubez, J.-C. Fontaine¹², D. Gelé, U. Goerlach, A.-C. Le Bihan, P. Van Hove

Centre de Calcul de l'Institut National de Physique Nucleaire et de Physique des Particules, CNRS/IN2P3, Villeurbanne, France

S. Gadrat

Université de Lyon, Université Claude Bernard Lyon 1, CNRS-IN2P3, Institut de Physique Nucléaire de Lyon, Villeurbanne, France

S. Beauceron, C. Bernet, G. Boudoul, C.A. Carrillo Montoya, R. Chierici, D. Contardo, B. Courbon, P. Depasse, H. El Mamouni, J. Fay, S. Gascon, M. Gouzevitch, G. Grenier, B. Ille, F. Lagarde, I.B. Laktineh, M. Lethuillier, L. Mirabito, A.L. Pequegnot, S. Perries, A. Popov¹³, D. Sabes, V. Sordini, M. Vander Donckt, P. Verdier, S. Viret

Georgian Technical University, Tbilisi, Georgia

A. Khvedelidze⁸

Tbilisi State University, Tbilisi, Georgia

D. Lomidze

RWTH Aachen University, I. Physikalisches Institut, Aachen, Germany

C. Autermann, S. Beranek, L. Feld, M.K. Kiesel, K. Klein, M. Lipinski, M. Preuten, C. Schomakers, J. Schulz, T. Verlage

RWTH Aachen University, III. Physikalisches Institut A, Aachen, Germany

A. Albert, M. Brodski, E. Dietz-Laursonn, D. Duchardt, M. Endres, M. Erdmann, S. Erdweg, T. Esch, R. Fischer, A. Güth, M. Hamer, T. Hebbeker, C. Heidemann, K. Hoepfner, S. Knutzen, M. Merschmeyer, A. Meyer, P. Millet, S. Mukherjee, M. Olschewski, K. Padeken, T. Pook, M. Radziej, H. Reithler, M. Rieger, F. Scheuch, L. Sonnenschein, D. Teyssier, S. Thüer

RWTH Aachen University, III. Physikalisches Institut B, Aachen, Germany

V. Cherepanov, G. Flügge, B. Kargoll, T. Kress, A. Künsken, J. Lingemann, T. Müller, A. Nehr Korn, A. Nowack, C. Pistone, O. Pooth, A. Stahl¹⁴

Deutsches Elektronen-Synchrotron, Hamburg, Germany

M. Aldaya Martin, T. Arndt, C. Asawatangtrakuldee, K. Beernaert, O. Behnke, U. Behrens, A.A. Bin Anuar, K. Borras¹⁵, A. Campbell, P. Connor, C. Contreras-Campana, F. Costanza, C. Diez Pardos, G. Dolinska, G. Eckerlin, D. Eckstein, T. Eichhorn, E. Eren, E. Gallo¹⁶, J. Garay Garcia, A. Geiser, A. Gizhko, J.M. Grados Luyando, A. Grohsjean, P. Gunnellini, A. Harb, J. Hauk, M. Hempel¹⁷, H. Jung, A. Kalogeropoulos, O. Karacheban¹⁷, M. Kasemann, J. Keaveney, C. Kleinwort, I. Korol, D. Krücker, W. Lange, A. Lelek, T. Lenz, J. Leonard, K. Lipka, A. Lobanov, W. Lohmann¹⁷, R. Mankel, I.-A. Melzer-Pellmann, A.B. Meyer, G. Mittag, J. Mnich, A. Mussgiller, D. Pitzl, R. Placakyte, A. Raspereza, B. Roland, M.Ö. Sahin, P. Saxena, T. Schoerner-Sadenius, S. Spannagel, N. Stefaniuk, G.P. Van Onsem, R. Walsh, C. Wissing

University of Hamburg, Hamburg, Germany

V. Blobel, M. Centis Vignali, A.R. Draeger, T. Dreyer, E. Garutti, D. Gonzalez, J. Haller, M. Hoffmann, A. Junkes, R. Klanner, R. Kogler, N. Kovalchuk, T. Lapsien, I. Marchesini, D. Marconi, M. Meyer, M. Niedziela, D. Nowatschin, F. Pantaleo¹⁴, T. Peiffer, A. Perieanu, C. Scharf, P. Schleper, A. Schmidt, S. Schumann, J. Schwandt, H. Stadie, G. Steinbrück, F.M. Stober, M. Stöver, H. Tholen, D. Troendle, E. Usai, L. Vanelderen, A. Vanhoefler, B. Vormwald

Institut für Experimentelle Kernphysik, Karlsruhe, Germany

M. Akbiyik, C. Barth, S. Baur, C. Baus, J. Berger, E. Butz, R. Caspart, T. Chwalek, F. Colombo, W. De Boer, A. Dierlamm, S. Fink, B. Freund, R. Friese, M. Giffels, A. Gilbert, P. Goldenzweig, D. Haitz, F. Hartmann¹⁴, S.M. Heindl, U. Husemann, I. Katkov¹³, S. Kudella, H. Mildner, M.U. Mozer, Th. Müller, M. Plagge, G. Quast, K. Rabbertz, S. Röcker, F. Roscher, M. Schröder, I. Shvetsov, G. Sieber, H.J. Simonis, R. Ulrich, S. Wayand, M. Weber, T. Weiler, S. Williamson, C. Wöhrmann, R. Wolf

Institute of Nuclear and Particle Physics (INPP), NCSR Demokritos, Aghia Paraskevi, Greece

G. Anagnostou, G. Daskalakis, T. Gerasis, V.A. Giakoumopoulou, A. Kyriakis, D. Loukas, I. Topsis-Giotis

National and Kapodistrian University of Athens, Athens, Greece

S. Kesisoglou, A. Panagiotou, N. Saoulidou, E. Tziaferi

University of Ioánnina, Ioánnina, Greece

I. Evangelou, G. Flouris, C. Foudas, P. Kokkas, N. Loukas, N. Manthos, I. Papadopoulos, E. Paradas

MTA-ELTE Lendület CMS Particle and Nuclear Physics Group, Eötvös Loránd University, Budapest, Hungary

N. Filipovic, G. Pasztor

Wigner Research Centre for Physics, Budapest, Hungary

G. Bencze, C. Hajdu, D. Horvath¹⁸, F. Sikler, V. Veszpremi, G. Vesztergombi¹⁹, A.J. Zsigmond

Institute of Nuclear Research ATOMKI, Debrecen, Hungary

N. Beni, S. Czellar, J. Karancsi²⁰, A. Makovec, J. Molnar, Z. Szillasi

Institute of Physics, University of Debrecen, Debrecen, Hungary

M. Bartók¹⁹, P. Raics, Z.L. Trocsanyi, B. Ujvari

Indian Institute of Science (IISc), Bangalore, India

J.R. Komaragiri

National Institute of Science Education and Research, Bhubaneswar, India

S. Bahinipati²¹, S. Bhowmik²², S. Choudhury²³, P. Mal, K. Mandal, A. Nayak²⁴, D.K. Sahoo²¹, N. Sahoo, S.K. Swain

Panjab University, Chandigarh, India

S. Bansal, S.B. Beri, V. Bhatnagar, U. Bhawandeep, R. Chawla, A.K. Kalsi, A. Kaur, M. Kaur, R. Kumar, P. Kumari, A. Mehta, M. Mittal, J.B. Singh, G. Walia

University of Delhi, Delhi, India

Ashok Kumar, A. Bhardwaj, B.C. Choudhary, R.B. Garg, S. Keshri, S. Malhotra, M. Naimuddin, K. Ranjan, R. Sharma, V. Sharma

Saha Institute of Nuclear Physics, HBNI, Kolkata, India

R. Bhattacharya, S. Bhattacharya, K. Chatterjee, S. Dey, S. Dutt, S. Dutta, S. Ghosh, N. Majumdar, A. Modak, K. Mondal, S. Mukhopadhyay, S. Nandan, A. Purohit, A. Roy, D. Roy, S. Roy Chowdhury, S. Sarkar, M. Sharan, S. Thakur

Indian Institute of Technology Madras, Madras, India

P.K. Behera

Bhabha Atomic Research Centre, Mumbai, India

R. Chudasama, D. Dutta, V. Jha, V. Kumar, A.K. Mohanty¹⁴, P.K. Netrakanti, L.M. Pant, P. Shukla, A. Topkar

Tata Institute of Fundamental Research-A, Mumbai, India

T. Aziz, S. Dugad, G. Kole, B. Mahakud, S. Mitra, G.B. Mohanty, B. Parida, N. Sur, B. Sutar

Tata Institute of Fundamental Research-B, Mumbai, India

S. Banerjee, R.K. Dewanjee, S. Ganguly, M. Guchait, Sa. Jain, S. Kumar, M. Maity²², G. Majumder, K. Mazumdar, T. Sarkar²², N. Wickramage²⁵

Indian Institute of Science Education and Research (IISER), Pune, India

S. Chauhan, S. Dube, V. Hegde, A. Kapoor, K. Kothekar, S. Pandey, A. Rane, S. Sharma

Institute for Research in Fundamental Sciences (IPM), Tehran, Iran

S. Chenarani²⁶, E. Eskandari Tadavani, S.M. Etesami²⁶, M. Khakzad, M. Mohammadi Najafabadi, M. Naseri, S. Paktinat Mehdiabadi²⁷, F. Rezaei Hosseinabadi, B. Safarzadeh²⁸, M. Zeinali

University College Dublin, Dublin, Ireland

M. Felcini, M. Grunewald

INFN Sezione di Bari ^a, Università di Bari ^b, Politecnico di Bari ^c, Bari, Italy

M. Abbrescia^{a,b}, C. Calabria^{a,b}, C. Caputo^{a,b}, A. Colaleo^a, D. Creanza^{a,c}, L. Cristella^{a,b}, N. De Filippis^{a,c}, M. De Palma^{a,b}, L. Fiore^a, G. Iaselli^{a,c}, G. Maggi^{a,c}, M. Maggi^a, G. Miniello^{a,b}, S. My^{a,b}, S. Nuzzo^{a,b}, A. Pompili^{a,b}, G. Pugliese^{a,c}, R. Radogna^{a,b}, A. Ranieri^a, G. Selvaggi^{a,b}, A. Sharma^a, L. Silvestris^{a,14}, R. Venditti^{a,b}, P. Verwilligen^a

INFN Sezione di Bologna ^a, Università di Bologna ^b, Bologna, Italy

G. Abbiendi^a, C. Battilana, D. Bonacorsi^{a,b}, S. Braibant-Giacomelli^{a,b}, L. Brigliadori^{a,b}, R. Campanini^{a,b}, P. Capiluppi^{a,b}, A. Castro^{a,b}, F.R. Cavallo^a, S.S. Chhibra^{a,b}, G. Codispoti^{a,b}, M. Cuffiani^{a,b}, G.M. Dallavalle^a, F. Fabbri^a, A. Fanfani^{a,b}, D. Fasanella^{a,b}, P. Giacomelli^a, C. Grandi^a, L. Guiducci^{a,b}, S. Marcellini^a, G. Masetti^a, A. Montanari^a, F.L. Navarria^{a,b}, A. Perrotta^a, A.M. Rossi^{a,b}, T. Rovelli^{a,b}, G.P. Siroli^{a,b}, N. Tosi^{a,b,14}

INFN Sezione di Catania ^a, Università di Catania ^b, Catania, Italy

S. Albergo^{a,b}, S. Costa^{a,b}, A. Di Mattia^a, F. Giordano^{a,b}, R. Potenza^{a,b}, A. Tricomi^{a,b}, C. Tuve^{a,b}

INFN Sezione di Firenze ^a, Università di Firenze ^b, Firenze, Italy

G. Barbagli^a, V. Ciulli^{a,b}, C. Civinini^a, R. D'Alessandro^{a,b}, E. Focardi^{a,b}, P. Lenzi^{a,b}, M. Meschini^a, S. Paoletti^a, L. Russo^{a,29}, G. Sguazzoni^a, D. Strom^a, L. Viliani^{a,b,14}

INFN Laboratori Nazionali di Frascati, Frascati, Italy

L. Benussi, S. Bianco, F. Fabbri, D. Piccolo, F. Primavera¹⁴

INFN Sezione di Genova ^a, Università di Genova ^b, Genova, Italy

V. Calvelli^{a,b}, F. Ferro^a, M.R. Monge^{a,b}, E. Robutti^a, S. Tosi^{a,b}

INFN Sezione di Milano-Bicocca ^a, Università di Milano-Bicocca ^b, Milano, Italy

L. Brianza^{a,b,14}, F. Brivio^{a,b}, V. Ciriolo, M.E. Dinardo^{a,b}, S. Fiorendi^{a,b,14}, S. Gennai^a, A. Ghezzi^{a,b}, P. Govoni^{a,b}, M. Malberti^{a,b}, S. Malvezzi^a, R.A. Manzoni^{a,b}, D. Menasce^a, L. Moroni^a, M. Paganoni^{a,b}, D. Pedrini^a, S. Pigazzini^{a,b}, S. Ragazzi^{a,b}, T. Tabarelli de Fatis^{a,b}

INFN Sezione di Napoli ^a, Università di Napoli 'Federico II' ^b, Napoli, Italy, Università della Basilicata ^c, Potenza, Italy, Università G. Marconi ^d, Roma, Italy

S. Buontempo^a, N. Cavallo^{a,c}, G. De Nardo, S. Di Guida^{a,d,14}, M. Esposito^{a,b}, F. Fabozzi^{a,c}, F. Fienga^{a,b}, A.O.M. Iorio^{a,b}, G. Lanza^a, L. Lista^a, S. Meola^{a,d,14}, P. Paolucci^{a,14}, C. Sciacca^{a,b}, F. Thyssen^a

INFN Sezione di Padova ^a, Università di Padova ^b, Padova, Italy, Università di Trento ^c, Trento, Italy

P. Azzi^{a,14}, N. Bacchetta^a, L. Benato^{a,b}, D. Bisello^{a,b}, A. Boletti^{a,b}, R. Carlin^{a,b}, A. Carvalho Antunes De Oliveira^{a,b}, P. Checchia^a, M. Dall'Osso^{a,b}, P. De Castro Manzano^a, T. Dorigo^a, F. Fanzago^a, F. Gasparini^{a,b}, F. Gonella^a, S. Lacaprara^a, M. Margoni^{a,b}, A.T. Meneguzzo^{a,b}, J. Pazzini^{a,b}, N. Pozzobon^{a,b}, P. Ronchese^{a,b}, F. Simonetto^{a,b}, E. Torassa^a, S. Ventura^a, M. Zanetti^{a,b}, P. Zotto^{a,b}, G. Zumerle^{a,b}

INFN Sezione di Pavia ^a, Università di Pavia ^b, Pavia, Italy

A. Braghieri^a, F. Fallavollita^{a,b}, A. Magnani^{a,b}, P. Montagna^{a,b}, S.P. Ratti^{a,b}, V. Re^a, C. Riccardi^{a,b}, P. Salvini^a, I. Vai^{a,b}, P. Vitulo^{a,b}

INFN Sezione di Perugia ^a, Università di Perugia ^b, Perugia, Italy

L. Alunni Solestizi^{a,b}, G.M. Bilei^a, D. Ciangottini^{a,b}, L. Fanò^{a,b}, P. Lariccia^{a,b}, R. Leonardi^{a,b}, G. Mantovani^{a,b}, V. Mariani^{a,b}, M. Menichelli^a, A. Saha^a, A. Santocchia^{a,b}

INFN Sezione di Pisa ^a, Università di Pisa ^b, Scuola Normale Superiore di Pisa ^c, Pisa, Italy

K. Androsov^{a,29}, P. Azzurri^{a,14}, G. Bagliesi^a, J. Bernardini^a, T. Boccali^a, R. Castaldi^a, M.A. Ciocci^{a,29}, R. Dell'Orso^a, S. Donato^{a,c}, G. Fedi, A. Giassi^a, M.T. Grippo^{a,29}, F. Ligabue^{a,c}, T. Lomtadze^a, L. Martini^{a,b}, A. Messineo^{a,b}, F. Palla^a, A. Rizzi^{a,b}, A. Savoy-Navarro^{a,30}, P. Spagnolo^a, R. Tenchini^a, G. Tonelli^{a,b}, A. Venturi^a, P.G. Verdini^a

INFN Sezione di Roma ^a, Sapienza Università di Roma ^b, Rome, Italy

L. Barone^{a,b}, F. Cavallari^a, M. Cipriani^{a,b}, D. Del Re^{a,b,14}, M. Diemoz^a, S. Gelli^{a,b}, E. Longo^{a,b}, F. Margaroli^{a,b}, B. Marzocchi^{a,b}, P. Meridiani^a, G. Organtini^{a,b}, R. Paramatti^a, F. Preiato^{a,b}, S. Rahatlou^{a,b}, C. Rovelli^a, F. Santanastasio^{a,b}

INFN Sezione di Torino ^a, Università di Torino ^b, Torino, Italy, Università del Piemonte Orientale ^c, Novara, Italy

N. Ampane^{a,b}, R. Arcidiacono^{a,c,14}, S. Argiro^{a,b}, M. Arneodo^{a,c}, N. Bartosik^a, R. Bellan^{a,b}, C. Biino^a, N. Cartiglia^a, F. Cenna^{a,b}, M. Costa^{a,b}, R. Covarelli^{a,b}, A. Degano^{a,b}, N. Demaria^a,

L. Finco^{a,b}, B. Kiani^{a,b}, C. Mariotti^a, S. Maselli^a, E. Migliore^{a,b}, V. Monaco^{a,b}, E. Monteil^{a,b}, M. Monteno^a, M.M. Obertino^{a,b}, L. Pacher^{a,b}, N. Pastrone^a, M. Pelliccioni^a, G.L. Pinna Angioni^{a,b}, F. Ravera^{a,b}, A. Romero^{a,b}, M. Ruspa^{a,c}, R. Sacchi^{a,b}, K. Shchelina^{a,b}, V. Sola^a, A. Solano^{a,b}, A. Staiano^a, P. Traczyk^{a,b}

INFN Sezione di Trieste^a, Università di Trieste^b, Trieste, Italy

S. Belforte^a, M. Casarsa^a, F. Cossutti^a, G. Della Ricca^{a,b}, A. Zanetti^a

Kyungpook National University, Daegu, Korea

D.H. Kim, G.N. Kim, M.S. Kim, S. Lee, S.W. Lee, Y.D. Oh, S. Sekmen, D.C. Son, Y.C. Yang

Chonbuk National University, Jeonju, Korea

A. Lee

Chonnam National University, Institute for Universe and Elementary Particles, Kwangju, Korea

H. Kim

Hanyang University, Seoul, Korea

J.A. Brochero Cifuentes, T.J. Kim

Korea University, Seoul, Korea

S. Cho, S. Choi, Y. Go, D. Gyun, S. Ha, B. Hong, Y. Jo, Y. Kim, K. Lee, K.S. Lee, S. Lee, J. Lim, S.K. Park, Y. Roh

Seoul National University, Seoul, Korea

J. Almond, J. Kim, H. Lee, S.B. Oh, B.C. Radburn-Smith, S.h. Seo, U.K. Yang, H.D. Yoo, G.B. Yu

University of Seoul, Seoul, Korea

M. Choi, H. Kim, J.H. Kim, J.S.H. Lee, I.C. Park, G. Ryu, M.S. Ryu

Sungkyunkwan University, Suwon, Korea

Y. Choi, J. Goh, C. Hwang, J. Lee, I. Yu

Vilnius University, Vilnius, Lithuania

V. Dudenas, A. Juodagalvis, J. Vaitkus

National Centre for Particle Physics, Universiti Malaya, Kuala Lumpur, Malaysia

I. Ahmed, Z.A. Ibrahim, M.A.B. Md Ali³¹, F. Mohamad Idris³², W.A.T. Wan Abdullah, M.N. Yusli, Z. Zolkapli

Centro de Investigacion y de Estudios Avanzados del IPN, Mexico City, Mexico

H. Castilla-Valdez, E. De La Cruz-Burelo, I. Heredia-De La Cruz³³, A. Hernandez-Almada, R. Lopez-Fernandez, R. Magaña Villalba, J. Mejia Guisao, A. Sanchez-Hernandez

Universidad Iberoamericana, Mexico City, Mexico

S. Carrillo Moreno, C. Oropeza Barrera, F. Vazquez Valencia

Benemerita Universidad Autonoma de Puebla, Puebla, Mexico

S. Carpinteyro, I. Pedraza, H.A. Salazar Ibarguen, C. Uribe Estrada

Universidad Autónoma de San Luis Potosí, San Luis Potosí, Mexico

A. Morelos Pineda

University of Auckland, Auckland, New Zealand

D. Krofcheck

University of Canterbury, Christchurch, New Zealand

P.H. Butler

National Centre for Physics, Quaid-I-Azam University, Islamabad, Pakistan

A. Ahmad, M. Ahmad, Q. Hassan, H.R. Hoorani, W.A. Khan, A. Saddique, M.A. Shah, M. Shoaib, M. Waqas

National Centre for Nuclear Research, Swierk, Poland

H. Bialkowska, M. Bluj, B. Boimska, T. Frueboes, M. Górski, M. Kazana, K. Nawrocki, K. Romanowska-Rybinska, M. Szleper, P. Zalewski

Institute of Experimental Physics, Faculty of Physics, University of Warsaw, Warsaw, Poland

K. Bunkowski, A. Byzuk³⁴, K. Doroba, A. Kalinowski, M. Konecki, J. Krolikowski, M. Misiura, M. Olszewski, M. Walczak

Laboratório de Instrumentação e Física Experimental de Partículas, Lisboa, Portugal

P. Bargassa, C. Beirão Da Cruz E Silva, B. Calpas, A. Di Francesco, P. Faccioli, P.G. Ferreira Parracho, M. Gallinaro, J. Hollar, N. Leonardo, L. Lloret Iglesias, M.V. Nemallapudi, J. Rodrigues Antunes, J. Seixas, O. Toldaiev, D. Vadrucio, J. Varela

Joint Institute for Nuclear Research, Dubna, Russia

S. Afanasiev, P. Bunin, M. Gavrilenko, I. Golutvin, I. Gorbunov, A. Kamenev, V. Karjavin, A. Lanev, A. Malakhov, V. Matveev^{35,36}, V. Palichik, V. Perelygin, S. Shmatov, S. Shulha, N. Skatchkov, V. Smirnov, N. Voytishin, A. Zarubin

Petersburg Nuclear Physics Institute, Gatchina (St. Petersburg), Russia

L. Chtchypounov, V. Golovtsov, Y. Ivanov, V. Kim³⁷, E. Kuznetsova³⁸, V. Murzin, V. Oreshkin, V. Sulimov, A. Vorobyev

Institute for Nuclear Research, Moscow, Russia

Yu. Andreev, A. Dermenev, S. Gninenko, N. Golubev, A. Karneyeu, M. Kirsanov, N. Krasnikov, A. Pashenkov, D. Tlisov, A. Toropin

Institute for Theoretical and Experimental Physics, Moscow, Russia

V. Epshteyn, V. Gavrillov, N. Lychkovskaya, V. Popov, I. Pozdnyakov, G. Safronov, A. Spiridonov, M. Toms, E. Vlasov, A. Zhokin

Moscow Institute of Physics and Technology, Moscow, Russia

T. Aushev, A. Bylinkin³⁶

National Research Nuclear University 'Moscow Engineering Physics Institute' (MEPhI), Moscow, Russia

R. Chistov³⁹, M. Danilov³⁹, V. Rusinov

P.N. Lebedev Physical Institute, Moscow, Russia

V. Andreev, M. Azarkin³⁶, I. Dremin³⁶, M. Kirakosyan, A. Leonidov³⁶, A. Terkulov

Skobeltsyn Institute of Nuclear Physics, Lomonosov Moscow State University, Moscow, Russia

A. Baskakov, A. Belyaev, E. Boos, V. Bunichev, M. Dubinin⁴⁰, L. Dudko, V. Klyukhin, O. Kodolova, N. Korneeva, I. Lokhtin, I. Miagkov, S. Obraztsov, M. Perfilov, V. Savrin, P. Volkov

Novosibirsk State University (NSU), Novosibirsk, Russia

V. Blinov⁴¹, Y. Skovpen⁴¹, D. Shtol⁴¹

State Research Center of Russian Federation, Institute for High Energy Physics, Protvino, Russia

I. Azhgirey, I. Bayshev, S. Bitioukov, D. Elumakhov, V. Kachanov, A. Kalinin, D. Konstantinov, V. Krychkine, V. Petrov, R. Ryutin, A. Sobol, S. Troshin, N. Tyurin, A. Uzunian, A. Volkov

University of Belgrade, Faculty of Physics and Vinca Institute of Nuclear Sciences, Belgrade, Serbia

P. Adzic⁴², P. Cirkovic, D. Devetak, M. Dordevic, J. Milosevic, V. Rekovic

Centro de Investigaciones Energéticas Medioambientales y Tecnológicas (CIEMAT), Madrid, Spain

J. Alcaraz Maestre, M. Barrio Luna, E. Calvo, M. Cerrada, M. Chamizo Llatas, N. Colino, B. De La Cruz, A. Delgado Peris, A. Escalante Del Valle, C. Fernandez Bedoya, J.P. Fernández Ramos, J. Flix, M.C. Fouz, P. Garcia-Abia, O. Gonzalez Lopez, S. Goy Lopez, J.M. Hernandez, M.I. Josa, E. Navarro De Martino, A. Pérez-Calero Yzquierdo, J. Puerta Pelayo, A. Quintario Olmeda, I. Redondo, L. Romero, M.S. Soares

Universidad Autónoma de Madrid, Madrid, Spain

J.F. de Trocóniz, M. Missiroli, D. Moran

Universidad de Oviedo, Oviedo, Spain

J. Cuevas, J. Fernandez Menendez, I. Gonzalez Caballero, J.R. González Fernández, E. Palencia Cortezon, S. Sanchez Cruz, I. Suárez Andrés, P. Vischia, J.M. Vizán Garcia

Instituto de Física de Cantabria (IFCA), CSIC-Universidad de Cantabria, Santander, Spain

I.J. Cabrillo, A. Calderon, E. Curras, M. Fernandez, J. Garcia-Ferrero, G. Gomez, A. Lopez Virto, J. Marco, C. Martinez Rivero, F. Matorras, J. Piedra Gomez, T. Rodrigo, A. Ruiz-Jimeno, L. Scodellaro, N. Trevisani, I. Vila, R. Vilar Cortabitarte

CERN, European Organization for Nuclear Research, Geneva, Switzerland

D. Abbaneo, E. Auffray, G. Auzinger, P. Baillon, A.H. Ball, D. Barney, P. Bloch, A. Bocci, C. Botta, T. Camporesi, R. Castello, M. Cepeda, G. Cerminara, Y. Chen, D. d'Enterria, A. Dabrowski, V. Daponte, A. David, M. De Gruttola, A. De Roeck, E. Di Marco⁴³, M. Dobson, B. Dorney, T. du Pree, D. Duggan, M. Dünser, N. Dupont, A. Elliott-Peisert, P. Everaerts, S. Fartoukh, G. Franzoni, J. Fulcher, W. Funk, D. Gigi, K. Gill, M. Girone, F. Glege, D. Gulhan, S. Gundacker, M. Guthoff, P. Harris, J. Hegeman, V. Innocente, P. Janot, J. Kieseler, H. Kirschenmann, V. Knünz, A. Kornmayer¹⁴, M.J. Kortelainen, K. Kousouris, M. Krammer¹, C. Lange, P. Lecoq, C. Lourenço, M.T. Lucchini, L. Malgeri, M. Mannelli, A. Martelli, F. Meijers, J.A. Merlin, S. Mersi, E. Meschi, P. Milenovic⁴⁴, F. Moortgat, S. Morovic, M. Mulders, H. Neugebauer, S. Orfanelli, L. Orsini, L. Pape, E. Perez, M. Peruzzi, A. Petrilli, G. Petrucciani, A. Pfeiffer, M. Pierini, A. Racz, T. Reis, G. Rolandi⁴⁵, M. Rovere, H. Sakulin, J.B. Sauvan, C. Schäfer, C. Schwick, M. Seidel, A. Sharma, P. Silva, P. Sphicas⁴⁶, J. Steggemann, M. Stoye, Y. Takahashi, M. Tosi, D. Treille, A. Triossi, A. Tsirou, V. Veckalns⁴⁷, G.I. Veres¹⁹, M. Verweij, N. Wardle, H.K. Wöhri, A. Zagozdinska³⁴, W.D. Zeuner

Paul Scherrer Institut, Villigen, Switzerland

W. Bertl, K. Deiters, W. Erdmann, R. Horisberger, Q. Ingram, H.C. Kaestli, D. Kotlinski, U. Langenegger, T. Rohe, S.A. Wiederkehr

Institute for Particle Physics, ETH Zurich, Zurich, Switzerland

F. Bachmair, L. Bäni, L. Bianchini, B. Casal, G. Dissertori, M. Dittmar, M. Donegà, C. Grab, C. Heidegger, D. Hits, J. Hoss, G. Kasieczka, W. Lustermann, B. Mangano, M. Marionneau, P. Martinez Ruiz del Arbol, M. Masciovecchio, M.T. Meinhard, D. Meister, F. Micheli,

P. Musella, F. Nessi-Tedaldi, F. Pandolfi, J. Pata, F. Pauss, G. Perrin, L. Perrozzi, M. Quittnat, M. Rossini, M. Schönenberger, A. Starodumov⁴⁸, V.R. Tavolaro, K. Theofilatos, R. Wallny

Universität Zürich, Zurich, Switzerland

T.K. Aarrestad, C. AMSler⁴⁹, L. Caminada, M.F. Canelli, A. De Cosa, C. Galloni, A. Hinzmann, T. Hreus, B. Kilminster, J. Ngadiuba, D. Pinna, G. Rauco, P. Robmann, D. Salerno, C. Seitz, Y. Yang, A. Zucchetta

National Central University, Chung-Li, Taiwan

V. Candelise, T.H. Doan, Sh. Jain, R. Khurana, M. Konyushikhin, C.M. Kuo, W. Lin, A. Pozdnyakov, S.S. Yu

National Taiwan University (NTU), Taipei, Taiwan

Arun Kumar, P. Chang, Y.H. Chang, Y. Chao, K.F. Chen, P.H. Chen, F. Fiori, W.-S. Hou, Y. Hsiung, Y.F. Liu, R.-S. Lu, M. Miñano Moya, E. Paganis, A. Psallidas, J.f. Tsai

Chulalongkorn University, Faculty of Science, Department of Physics, Bangkok, Thailand

B. Asavapibhop, G. Singh, N. Srimanobhas, N. Suwonjandee

Cukurova University, Physics Department, Science and Art Faculty, Adana, Turkey

A. Adiguzel, S. Cerci⁵⁰, S. Damarseckin, Z.S. Demiroglu, C. Dozen, I. Dumanoglu, S. Girgis, G. Gokbulut, Y. Guler, I. Hos⁵¹, E.E. Kangal⁵², O. Kara, U. Kiminsu, M. Oglakci, G. Onengut⁵³, K. Ozdemir⁵⁴, D. Sunar Cerci⁵⁰, B. Tali⁵⁰, H. Topakli⁵⁵, S. Turkcapar, I.S. Zorbakir, C. Zorbilmez

Middle East Technical University, Physics Department, Ankara, Turkey

B. Bilin, S. Bilmis, B. Isildak⁵⁶, G. Karapinar⁵⁷, M. Yalvac, M. Zeyrek

Bogazici University, Istanbul, Turkey

E. Gülmez, M. Kaya⁵⁸, O. Kaya⁵⁹, E.A. Yetkin⁶⁰, T. Yetkin⁶¹

Istanbul Technical University, Istanbul, Turkey

A. Cakir, K. Cankocak, S. Sen⁶²

Institute for Scintillation Materials of National Academy of Science of Ukraine, Kharkov, Ukraine

B. Grynyov

National Scientific Center, Kharkov Institute of Physics and Technology, Kharkov, Ukraine

L. Levchuk, P. Sorokin

University of Bristol, Bristol, United Kingdom

R. Aggleton, F. Ball, L. Beck, J.J. Brooke, D. Burns, E. Clement, D. Cussans, H. Flacher, J. Goldstein, M. Grimes, G.P. Heath, H.F. Heath, J. Jacob, L. Kreczko, C. Lucas, D.M. Newbold⁶³, S. Paramesvaran, A. Poll, T. Sakuma, S. Seif El Nasr-storey, D. Smith, V.J. Smith

Rutherford Appleton Laboratory, Didcot, United Kingdom

K.W. Bell, A. Belyaev⁶⁴, C. Brew, R.M. Brown, L. Calligaris, D. Cieri, D.J.A. Cockerill, J.A. Coughlan, K. Harder, S. Harper, E. Olaiya, D. Petyt, C.H. Shepherd-Themistocleous, A. Thea, I.R. Tomalin, T. Williams

Imperial College, London, United Kingdom

M. Baber, R. Bainbridge, O. Buchmuller, A. Bundock, D. Burton, S. Casasso, M. Citron, D. Colling, L. Corpe, P. Dauncey, G. Davies, A. De Wit, M. Della Negra, R. Di Maria, P. Dunne, A. Elwood, D. Futyan, Y. Haddad, G. Hall, G. Iles, T. James, R. Lane, C. Laner, R. Lucas⁶³, L. Lyons, A.-M. Magnan, S. Malik, L. Mastrolorenzo, J. Nash, A. Nikitenko⁴⁸, J. Pela, B. Penning,

M. Pesaresi, D.M. Raymond, A. Richards, A. Rose, E. Scott, C. Seez, S. Summers, A. Tapper, K. Uchida, M. Vazquez Acosta⁶⁵, T. Virdee¹⁴, J. Wright, S.C. Zenz

Brunel University, Uxbridge, United Kingdom

J.E. Cole, P.R. Hobson, A. Khan, P. Kyberd, I.D. Reid, P. Symonds, L. Teodorescu, M. Turner

Baylor University, Waco, USA

A. Borzou, K. Call, J. Dittmann, K. Hatakeyama, H. Liu, N. Pastika

Catholic University of America, Washington, USA

R. Bartek, A. Dominguez

The University of Alabama, Tuscaloosa, USA

A. Buccilli, S.I. Cooper, C. Henderson, P. Rumerio, C. West

Boston University, Boston, USA

D. Arcaro, A. Avetisyan, T. Bose, D. Gastler, D. Rankin, C. Richardson, J. Rohlf, L. Sulak, D. Zou

Brown University, Providence, USA

G. Benelli, D. Cutts, A. Garabedian, J. Hakala, U. Heintz, J.M. Hogan, O. Jesus, K.H.M. Kwok, E. Laird, G. Landsberg, Z. Mao, M. Narain, S. Piperov, S. Sagir, E. Spencer, R. Syarif

University of California, Davis, Davis, USA

R. Breedon, D. Burns, M. Calderon De La Barca Sanchez, S. Chauhan, M. Chertok, J. Conway, R. Conway, P.T. Cox, R. Erbacher, C. Flores, G. Funk, M. Gardner, W. Ko, R. Lander, C. Mclean, M. Mulhearn, D. Pellett, J. Pilot, S. Shalhout, M. Shi, J. Smith, M. Squires, D. Stolp, K. Tos, M. Tripathi

University of California, Los Angeles, USA

M. Bachtis, C. Bravo, R. Cousins, A. Dasgupta, A. Florent, J. Hauser, M. Ignatenko, N. Mccoll, D. Saltzberg, C. Schnaible, V. Valuev, M. Weber

University of California, Riverside, Riverside, USA

E. Bouvier, K. Burt, R. Clare, J. Ellison, J.W. Gary, S.M.A. Ghiasi Shirazi, G. Hanson, J. Heilman, P. Jandir, E. Kennedy, F. Lacroix, O.R. Long, M. Olmedo Negrete, M.I. Paneva, A. Shrinivas, W. Si, H. Wei, S. Wimpenny, B. R. Yates

University of California, San Diego, La Jolla, USA

J.G. Branson, G.B. Cerati, S. Cittolin, M. Derdzinski, R. Gerosa, A. Holzner, D. Klein, V. Krutelyov, J. Letts, I. Macneill, D. Olivito, S. Padhi, M. Pieri, M. Sani, V. Sharma, S. Simon, M. Tadel, A. Vartak, S. Wasserbaech⁶⁶, C. Welke, J. Wood, F. Würthwein, A. Yagil, G. Zevi Della Porta

University of California, Santa Barbara - Department of Physics, Santa Barbara, USA

N. Amin, R. Bhandari, J. Bradmiller-Feld, C. Campagnari, A. Dishaw, V. Dutta, M. Franco Sevilla, C. George, F. Golf, L. Gouskos, J. Gran, R. Heller, J. Incandela, S.D. Mullin, A. Ovcharova, H. Qu, J. Richman, D. Stuart, I. Suarez, J. Yoo

California Institute of Technology, Pasadena, USA

D. Anderson, J. Bendavid, A. Bornheim, J. Bunn, J. Duarte, J.M. Lawhorn, A. Mott, H.B. Newman, C. Pena, M. Spiropulu, J.R. Vlimant, S. Xie, R.Y. Zhu

Carnegie Mellon University, Pittsburgh, USA

M.B. Andrews, T. Ferguson, M. Paulini, J. Russ, M. Sun, H. Vogel, I. Vorobiev, M. Weinberg

University of Colorado Boulder, Boulder, USA

J.P. Cumalat, W.T. Ford, F. Jensen, A. Johnson, M. Krohn, S. Leontsinis, T. Mulholland, K. Stenson, S.R. Wagner

Cornell University, Ithaca, USA

J. Alexander, J. Chaves, J. Chu, S. Dittmer, K. Mcdermott, N. Mirman, G. Nicolas Kaufman, J.R. Patterson, A. Rinkevicius, A. Ryd, L. Skinnari, L. Soffi, S.M. Tan, Z. Tao, J. Thom, J. Tucker, P. Wittich, M. Zientek

Fairfield University, Fairfield, USA

D. Winn

Fermi National Accelerator Laboratory, Batavia, USA

S. Abdullin, M. Albrow, G. Apollinari, A. Apresyan, S. Banerjee, L.A.T. Bauerdick, A. Beretvas, J. Berryhill, P.C. Bhat, G. Bolla, K. Burkett, J.N. Butler, H.W.K. Cheung, F. Chlebana, S. Cihangir[†], M. Cremonesi, V.D. Elvira, I. Fisk, J. Freeman, E. Gottschalk, L. Gray, D. Green, S. Grünendahl, O. Gutsche, D. Hare, R.M. Harris, S. Hasegawa, J. Hirschauer, Z. Hu, B. Jayatilaka, S. Jindariani, M. Johnson, U. Joshi, B. Klima, B. Kreis, S. Lammel, J. Linacre, D. Lincoln, R. Lipton, M. Liu, T. Liu, R. Lopes De Sá, J. Lykken, K. Maeshima, N. Magini, J.M. Marraffino, S. Maruyama, D. Mason, P. McBride, P. Merkel, S. Mrenna, S. Nahn, V. O'Dell, K. Pedro, O. Prokofyev, G. Rakness, L. Ristori, E. Sexton-Kennedy, A. Soha, W.J. Spalding, L. Spiegel, S. Stoynev, J. Strait, N. Strobbe, L. Taylor, S. Tkaczyk, N.V. Tran, L. Uplegger, E.W. Vaandering, C. Vernieri, M. Verzocchi, R. Vidal, M. Wang, H.A. Weber, A. Whitbeck, Y. Wu

University of Florida, Gainesville, USA

D. Acosta, P. Avery, P. Bortignon, D. Bourilkov, A. Brinkerhoff, A. Carnes, M. Carver, D. Curry, S. Das, R.D. Field, I.K. Furic, J. Konigsberg, A. Korytov, J.F. Low, P. Ma, K. Matchev, H. Mei, G. Mitselmakher, D. Rank, L. Shchutska, D. Sperka, L. Thomas, J. Wang, S. Wang, J. Yelton

Florida International University, Miami, USA

S. Linn, P. Markowitz, G. Martinez, J.L. Rodriguez

Florida State University, Tallahassee, USA

A. Ackert, T. Adams, A. Askew, S. Bein, S. Hagopian, V. Hagopian, K.F. Johnson, T. Kolberg, H. Prosper, A. Santra, R. Yohay

Florida Institute of Technology, Melbourne, USA

M.M. Baarmand, V. Bhopatkar, S. Colafranceschi, M. Hohlmann, D. Noonan, T. Roy, F. Yumiceva

University of Illinois at Chicago (UIC), Chicago, USA

M.R. Adams, L. Apanasevich, D. Berry, R.R. Betts, I. Bucinskaite, R. Cavanaugh, O. Evdokimov, L. Gauthier, C.E. Gerber, D.J. Hofman, K. Jung, I.D. Sandoval Gonzalez, N. Varelas, H. Wang, Z. Wu, M. Zakaria, J. Zhang

The University of Iowa, Iowa City, USA

B. Bilki⁶⁷, W. Clarida, K. Dilsiz, S. Durgut, R.P. Gandrajula, M. Haytmyradov, V. Khristenko, J.-P. Merlo, H. Mermerkaya⁶⁸, A. Mestvirishvili, A. Moeller, J. Nachtman, H. Ogul, Y. Onel, F. Ozok⁶⁹, A. Penzo, C. Snyder, E. Tiras, J. Wetzel, K. Yi

Johns Hopkins University, Baltimore, USA

B. Blumenfeld, A. Cocoros, N. Eminizer, D. Fehling, L. Feng, A.V. Gritsan, P. Maksimovic, J. Roskes, U. Sarica, M. Swartz, M. Xiao, C. You

The University of Kansas, Lawrence, USA

A. Al-bataineh, P. Baringer, A. Bean, S. Boren, J. Bowen, J. Castle, L. Forthomme, R.P. Kenny III, S. Khalil, A. Kropivnitskaya, D. Majumder, W. Mcbrayer, M. Murray, S. Sanders, R. Stringer, J.D. Tapia Takaki, Q. Wang

Kansas State University, Manhattan, USA

A. Ivanov, K. Kaadze, Y. Maravin, A. Mohammadi, L.K. Saini, N. Skhirtladze, S. Toda

Lawrence Livermore National Laboratory, Livermore, USA

F. Rebassoo, D. Wright

University of Maryland, College Park, USA

C. Anelli, A. Baden, O. Baron, A. Belloni, B. Calvert, S.C. Eno, C. Ferraioli, J.A. Gomez, N.J. Hadley, S. Jabeen, G.Y. Jeng, R.G. Kellogg, J. Kunkle, A.C. Mignerey, F. Ricci-Tam, Y.H. Shin, A. Skuja, M.B. Tonjes, S.C. Tonwar

Massachusetts Institute of Technology, Cambridge, USA

D. Abercrombie, B. Allen, A. Apyan, V. Azzolini, R. Barbieri, A. Baty, R. Bi, K. Bierwagen, S. Brandt, W. Busza, I.A. Cali, M. D'Alfonso, Z. Demiragli, G. Gomez Ceballos, M. Goncharov, D. Hsu, Y. Iiyama, G.M. Innocenti, M. Klute, D. Kovalskyi, K. Krajczar, Y.S. Lai, Y.-J. Lee, A. Levin, P.D. Luckey, B. Maier, A.C. Marini, C. McGinn, C. Mironov, S. Narayanan, X. Niu, C. Paus, C. Roland, G. Roland, J. Salfeld-Nebgen, G.S.F. Stephans, K. Tatar, D. Velicanu, J. Wang, T.W. Wang, B. Wyslouch

University of Minnesota, Minneapolis, USA

A.C. Benvenuti, R.M. Chatterjee, A. Evans, P. Hansen, S. Kalafut, S.C. Kao, Y. Kubota, Z. Lesko, J. Mans, S. Nourbakhsh, N. Ruckstuhl, R. Rusack, N. Tambe, J. Turkewitz

University of Mississippi, Oxford, USA

J.G. Acosta, S. Oliveros

University of Nebraska-Lincoln, Lincoln, USA

E. Avdeeva, K. Bloom, D.R. Claes, C. Fangmeier, R. Gonzalez Suarez, R. Kamalieddin, I. Kravchenko, A. Malta Rodrigues, J. Monroy, J.E. Siado, G.R. Snow, B. Stieger

State University of New York at Buffalo, Buffalo, USA

M. Alyari, J. Dolen, A. Godshalk, C. Harrington, I. Iashvili, J. Kaisen, D. Nguyen, A. Parker, S. Rappoccio, B. Roozbahani

Northeastern University, Boston, USA

G. Alverson, E. Barberis, A. Hortiangtham, A. Massironi, D.M. Morse, D. Nash, T. Orimoto, R. Teixeira De Lima, D. Trocino, R.-J. Wang, D. Wood

Northwestern University, Evanston, USA

S. Bhattacharya, O. Charaf, K.A. Hahn, A. Kumar, N. Mucia, N. Odell, B. Pollack, M.H. Schmitt, K. Sung, M. Trovato, M. Velasco

University of Notre Dame, Notre Dame, USA

N. Dev, M. Hildreth, K. Hurtado Anampa, C. Jessop, D.J. Karmgard, N. Kellams, K. Lannon, N. Marinelli, F. Meng, C. Mueller, Y. Musienko³⁵, M. Planer, A. Reinsvold, R. Ruchti, N. Rupperecht, G. Smith, S. Taroni, M. Wayne, M. Wolf, A. Woodard

The Ohio State University, Columbus, USA

J. Alimena, L. Antonelli, B. Bylsma, L.S. Durkin, S. Flowers, B. Francis, A. Hart, C. Hill, R. Hughes, W. Ji, B. Liu, W. Luo, D. Puigh, B.L. Winer, H.W. Wulsin

Princeton University, Princeton, USA

S. Cooperstein, O. Driga, P. Elmer, J. Hardenbrook, P. Hebda, D. Lange, J. Luo, D. Marlow, T. Medvedeva, K. Mei, I. Ojalvo, J. Olsen, C. Palmer, P. Piroué, D. Stickland, A. Svyatkovskiy, C. Tully

University of Puerto Rico, Mayaguez, USA

S. Malik

Purdue University, West Lafayette, USA

A. Barker, V.E. Barnes, S. Folgueras, L. Gutay, M.K. Jha, M. Jones, A.W. Jung, A. Khatiwada, D.H. Miller, N. Neumeister, J.F. Schulte, X. Shi, J. Sun, F. Wang, W. Xie

Purdue University Northwest, Hammond, USA

N. Parashar, J. Stupak

Rice University, Houston, USA

A. Adair, B. Akgun, Z. Chen, K.M. Ecklund, F.J.M. Geurts, M. Guilbaud, W. Li, B. Michlin, M. Northup, B.P. Padley, J. Roberts, J. Rorie, Z. Tu, J. Zabel

University of Rochester, Rochester, USA

B. Betchart, A. Bodek, P. de Barbaro, R. Demina, Y.t. Duh, T. Ferbel, M. Galanti, A. Garcia-Bellido, J. Han, O. Hindrichs, A. Khukhunaishvili, K.H. Lo, P. Tan, M. Verzetti

Rutgers, The State University of New Jersey, Piscataway, USA

A. Agapitos, J.P. Chou, Y. Gershtein, T.A. Gómez Espinosa, E. Halkiadakis, M. Heindl, E. Hughes, S. Kaplan, R. Kunnawalkam Elayavalli, S. Kyriacou, A. Lath, K. Nash, M. Osherson, H. Saka, S. Salur, S. Schnetzer, D. Sheffield, S. Somalwar, R. Stone, S. Thomas, P. Thomassen, M. Walker

University of Tennessee, Knoxville, USA

A.G. Delannoy, M. Foerster, J. Heideman, G. Riley, K. Rose, S. Spanier, K. Thapa

Texas A&M University, College Station, USA

O. Bouhali⁷⁰, A. Celik, M. Dalchenko, M. De Mattia, A. Delgado, S. Dildick, R. Eusebi, J. Gilmore, T. Huang, E. Juska, T. Kamon⁷¹, R. Mueller, Y. Pakhotin, R. Patel, A. Perloff, L. Perniè, D. Rathjens, A. Safonov, A. Tatarinov, K.A. Ulmer

Texas Tech University, Lubbock, USA

N. Akchurin, J. Damgov, F. De Guio, C. Dragoiu, P.R. Duderø, J. Faulkner, E. Gurpinar, S. Kunori, K. Lamichhane, S.W. Lee, T. Libeiro, T. Peltola, S. Undleeb, I. Volobouev, Z. Wang

Vanderbilt University, Nashville, USA

S. Greene, A. Gurrola, R. Janjam, W. Johns, C. Maguire, A. Melo, H. Ni, P. Sheldon, S. Tuo, J. Velkovska, Q. Xu

University of Virginia, Charlottesville, USA

M.W. Arenton, P. Barria, B. Cox, J. Goodell, R. Hirosky, A. Ledovskoy, H. Li, C. Neu, T. Sinthuprasith, X. Sun, Y. Wang, E. Wolfe, F. Xia

Wayne State University, Detroit, USA

C. Clarke, R. Harr, P.E. Karchin, J. Sturdy

University of Wisconsin - Madison, Madison, WI, USA

D.A. Belknap, J. Buchanan, C. Caillol, S. Dasu, L. Dodd, S. Duric, B. Gomber, M. Grothe, M. Herndon, A. Hervé, P. Klabbbers, A. Lanaro, A. Levine, K. Long, R. Loveless, T. Perry, G.A. Pierro, G. Polese, T. Ruggles, A. Savin, N. Smith, W.H. Smith, D. Taylor, N. Woods

†: Deceased

- 1: Also at Vienna University of Technology, Vienna, Austria
- 2: Also at State Key Laboratory of Nuclear Physics and Technology, Peking University, Beijing, China
- 3: Also at Institut Pluridisciplinaire Hubert Curien (IPHC), Université de Strasbourg, CNRS/IN2P3, Strasbourg, France
- 4: Also at Universidade Estadual de Campinas, Campinas, Brazil
- 5: Also at Universidade Federal de Pelotas, Pelotas, Brazil
- 6: Also at Université Libre de Bruxelles, Bruxelles, Belgium
- 7: Also at Deutsches Elektronen-Synchrotron, Hamburg, Germany
- 8: Also at Joint Institute for Nuclear Research, Dubna, Russia
- 9: Now at Ain Shams University, Cairo, Egypt
- 10: Now at British University in Egypt, Cairo, Egypt
- 11: Also at Zewail City of Science and Technology, Zewail, Egypt
- 12: Also at Université de Haute Alsace, Mulhouse, France
- 13: Also at Skobeltsyn Institute of Nuclear Physics, Lomonosov Moscow State University, Moscow, Russia
- 14: Also at CERN, European Organization for Nuclear Research, Geneva, Switzerland
- 15: Also at RWTH Aachen University, III. Physikalisches Institut A, Aachen, Germany
- 16: Also at University of Hamburg, Hamburg, Germany
- 17: Also at Brandenburg University of Technology, Cottbus, Germany
- 18: Also at Institute of Nuclear Research ATOMKI, Debrecen, Hungary
- 19: Also at MTA-ELTE Lendület CMS Particle and Nuclear Physics Group, Eötvös Loránd University, Budapest, Hungary
- 20: Also at Institute of Physics, University of Debrecen, Debrecen, Hungary
- 21: Also at Indian Institute of Technology Bhubaneswar, Bhubaneswar, India
- 22: Also at University of Visva-Bharati, Santiniketan, India
- 23: Also at Indian Institute of Science Education and Research, Bhopal, India
- 24: Also at Institute of Physics, Bhubaneswar, India
- 25: Also at University of Ruhuna, Matara, Sri Lanka
- 26: Also at Isfahan University of Technology, Isfahan, Iran
- 27: Also at Yazd University, Yazd, Iran
- 28: Also at Plasma Physics Research Center, Science and Research Branch, Islamic Azad University, Tehran, Iran
- 29: Also at Università degli Studi di Siena, Siena, Italy
- 30: Also at Purdue University, West Lafayette, USA
- 31: Also at International Islamic University of Malaysia, Kuala Lumpur, Malaysia
- 32: Also at Malaysian Nuclear Agency, MOSTI, Kajang, Malaysia
- 33: Also at Consejo Nacional de Ciencia y Tecnología, Mexico city, Mexico
- 34: Also at Warsaw University of Technology, Institute of Electronic Systems, Warsaw, Poland
- 35: Also at Institute for Nuclear Research, Moscow, Russia
- 36: Now at National Research Nuclear University 'Moscow Engineering Physics Institute' (MEPhI), Moscow, Russia
- 37: Also at St. Petersburg State Polytechnical University, St. Petersburg, Russia
- 38: Also at University of Florida, Gainesville, USA
- 39: Also at P.N. Lebedev Physical Institute, Moscow, Russia
- 40: Also at California Institute of Technology, Pasadena, USA
- 41: Also at Budker Institute of Nuclear Physics, Novosibirsk, Russia
- 42: Also at Faculty of Physics, University of Belgrade, Belgrade, Serbia

-
- 43: Also at INFN Sezione di Roma; Sapienza Università di Roma, Rome, Italy
- 44: Also at University of Belgrade, Faculty of Physics and Vinca Institute of Nuclear Sciences, Belgrade, Serbia
- 45: Also at Scuola Normale e Sezione dell'INFN, Pisa, Italy
- 46: Also at National and Kapodistrian University of Athens, Athens, Greece
- 47: Also at Riga Technical University, Riga, Latvia
- 48: Also at Institute for Theoretical and Experimental Physics, Moscow, Russia
- 49: Also at Albert Einstein Center for Fundamental Physics, Bern, Switzerland
- 50: Also at Adiyaman University, Adiyaman, Turkey
- 51: Also at Istanbul Aydin University, Istanbul, Turkey
- 52: Also at Mersin University, Mersin, Turkey
- 53: Also at Cag University, Mersin, Turkey
- 54: Also at Piri Reis University, Istanbul, Turkey
- 55: Also at Gaziosmanpasa University, Tokat, Turkey
- 56: Also at Ozyegin University, Istanbul, Turkey
- 57: Also at Izmir Institute of Technology, Izmir, Turkey
- 58: Also at Marmara University, Istanbul, Turkey
- 59: Also at Kafkas University, Kars, Turkey
- 60: Also at Istanbul Bilgi University, Istanbul, Turkey
- 61: Also at Yildiz Technical University, Istanbul, Turkey
- 62: Also at Hacettepe University, Ankara, Turkey
- 63: Also at Rutherford Appleton Laboratory, Didcot, United Kingdom
- 64: Also at School of Physics and Astronomy, University of Southampton, Southampton, United Kingdom
- 65: Also at Instituto de Astrofísica de Canarias, La Laguna, Spain
- 66: Also at Utah Valley University, Orem, USA
- 67: Also at Argonne National Laboratory, Argonne, USA
- 68: Also at Erzincan University, Erzincan, Turkey
- 69: Also at Mimar Sinan University, Istanbul, Istanbul, Turkey
- 70: Also at Texas A&M University at Qatar, Doha, Qatar
- 71: Also at Kyungpook National University, Daegu, Korea